Energy Conversion and Management 114 (2016) 50–67

Contents lists available at ScienceDirect

Energy Conversion and Management

journal homepage: www.elsevier.com/locate/enconman

Review

Key issues in development of thermoelectric power generators: High figure-of-merit materials and their highly conducting interfaces with metallic interconnects

Dinesh K. Aswal [a,b,*], Ranita Basu [a], Ajay Singh [a,*]

[a] Technical Physics Division, Bhabha Atomic Research Center, Mumbai 400 085, India
[b] National Physical Laboratory, Dr. K.S. Krishnan Road, New Delhi 110012, India

ARTICLE INFO

Article history:
Received 30 November 2015
Accepted 27 January 2016

Keywords:
Thermoelectrics
Seebeck effect
Interfaces
Specific contact resistance
Efficiency
Thermal conductivity

ABSTRACT

Thermoelectric generators (TEGs) are devices that convert temperature differences into electrical energy, which work on the thermoelectric phenomena known as Seebeck effect. The thermoelectric phenomena have widely been used for heating and cooling applications, however electric power generation has only been limited to niche applications e.g. thermoelectric power generators for space missions. TEG provides one of cleanest energy conversion method, which is noise-free, virtually maintenance free and can continuously produces power for several years under ambient conditions. In recent years, energy generation through thermoelectric harvesting has witnessed an increased interest for various applications, including tapping waste heat from the exhaust of vehicles, from industries, etc. The development of an efficient TEG requires the fulfillment of several factors, which includes availability of n- and p-type thermoelectric materials with high figure-of-merit (*ZT*), preparation of ohmic contacts between thermoelements and metallic interconnects and management of maximum heat transfer though the device. In this review, we present an overview on the various aspects of device development i.e. from synthesis of high *ZT* thermoelectric materials to issues & design aspects of the TEG. A discussion on the various strategies employed to improve *ZT* is described. It is shown that a *ZT* of >2 has widely been reported in literature, which has been achieved either by enhancing the power factor and/or reducing the thermal conductivity of the materials. A discussion on the status on the development of TEGs suitable for operation at different temperature ranges i.e. <250 °C, 250–650 °C and >650 °C is presented. Finally, the cost of fabrication of TEGs and their potential applications in different areas have been highlighted.

Contents

* Corresponding authors at: Technical Physics Division, Bhabha Atomic Research Center, Mumbai 400 085, India (D.K. Aswal and A. Singh).
E-mail addresses: dkaswal@yahoo.com (D.K. Aswal), asb_barc@yahoo.com (A. Singh).

http://dx.doi.org/10.1016/j.enconman.2016.01.065
0196-8904/

1. Introduction

Thermoelectric power generators (TEGs) convert heat directly into electricity without requiring any moving components that make them ideal for small scale power generation. A TEG essentially consist of a large number of p-type and n-type thermoelements connected alternately electrically in series and thermally in parallel [1,2]. A temperature difference between hot and cold ends of the TEG produces a voltage via Seebeck effect. The waste heat from different sources can be supplied to the hot side of the TEG, which is rejected at a lower temperature from the cold side (or heat sink) of the device. Thus the electricity produced by the TEGs from waste heat can be economic if their production cost is lowered.

Nearly 70% of world energy is known to be wasted as heat which is dissipated in the atmosphere and is considered as one of the factors for global warming [3]. Thus reutilization of waste heat into electricity using TEGs are beneficial for energy savings as well as for environment. Various sources that generate waste heat – depending upon the temperature generated by them – can broadly be classified into following three categories [1–5]:

(i) low temperature source (<250 °C): the major sources in this temperature range include air-conditioning/refrigeration condenser, ovens, air compressors, furnace doors, electronic circuit, etc.
(ii) mid temperature source (~250–650 °C): the sources for this temperature include steam boiler exhaust, gas turbine exhaust, drying & baking ovens, automotive exhaust, etc.
(iii) high temperature source (>650 °C): the sources for this temperature region include metal refining furnaces, steel heating furnace, hydrogen plants, etc. The natural decay of the radio-isotopes (such as Pu^{238}) also produces high temperature heat (~800–1000 °C) and TEG utilizing heat sources are named as radio-isotope thermoelectric power generators (RTG).

Owing to the lower efficiencies and high costs, the applications of TEGs has long been restricted to the RTG for space missions [1]. However, during past two decades a wide variety of new materials exhibiting high thermoelectric performance over a wide temperature range have been discovered. These include, new chalcogenides and their composites, skutterudites, clathrates, half Heuslers, zintl, oxides, and organic semiconductors [6]. The advent of high performance thermoelectric materials along with a need to recover power from various waste heat sources have increased the interest in fabrication of efficient TEGs [6]. However, conversions of high performance materials into efficient TEGs has been marred by the complexities involved in the preparation of high quality electrical and thermal interfaces. Nevertheless, there have been serious attempts in literature to fabricate efficient TEGs, which are operable at different temperatures. This review is aimed to comprehend the current status on the development of TEGs suitable for different temperature ranges. The major issues touched upon include design of TEG, new approaches employed for the enhancement of ZT of thermoelectric materials via tailoring the thermal and electrical transport properties and fabrication of low electrical contact resistances. A brief discussion on the economic viability of TEGs and their applications in different areas is presented.

2. Engineering aspect of TEG development

Extracting the electrical power from a thermoelectric material primarily depends on the design engineering of the TEG. A typical schematic diagram showing the internal architecture of TEG is presented in Fig. 1. In a TEG, several p- and n-type thermoelements are joined electrically in series and thermally in parallel, which at outset looks too simple. However, in practice the design of TEG is more complex as one has to consider the efficient electric and thermal transports. Therefore, in order to fabricate high efficiency (η) TEG, the technological challenges are to prepare various electrical contacts which not only are ohmic in nature but also have the lowest possible value of contact resistance (i.e. the value of contact resistance should be far less than the bulk resistance of the thermoelement). Similarly, one should able to prepare thermal contact close to ideality i.e. almost all the heat flows through the thermoelements and the heat flow through the shunt-path is nearly zero. However, in reality the preparations of ideal electrical and thermal contacts are very difficult. In addition, the η of TEG is defined through the relation [1,2]:

$$\eta = \frac{T_h - T_c}{T_h}\left(\frac{\sqrt{1+ZT_{avg}}-1}{\sqrt{1+ZT_{avg}}+T_c/T_h}\right) \quad (1)$$

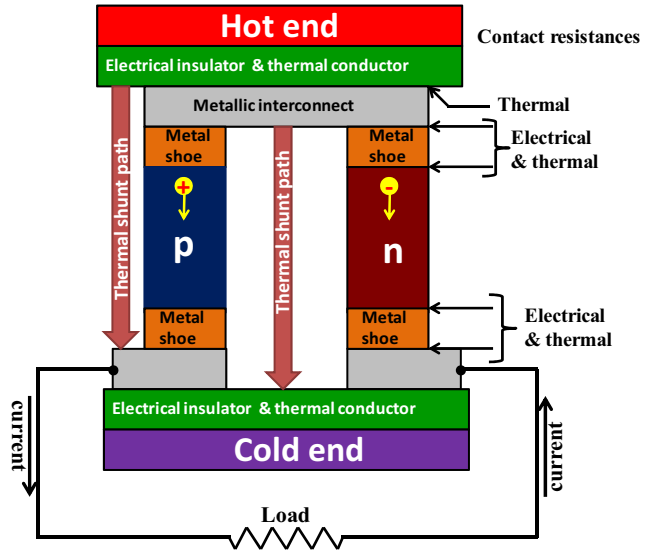

Fig. 1. Schematic of the internal architecture of a single p–n leg based thermoelectric power generator showing different electrical and thermal interfaces.

Here T_h and T_c are respective hot end and cold end temperature of thermoelectric materials and T_{avg} is the average temperature of T_h and T_c. The ZT_{avg} is the average figure-of-merit for each thermoelement and it is defined as [1,2]:

$$ZT_{avg} = \alpha^2 \sigma T/\kappa \quad (2)$$

Here α is the Seebeck coefficient, σ is the electrical conductivity and κ is the thermal conductivity of each thermoelement. To achieve high efficiency, it is very important to use materials with high ZT_{avg}. Large α (to have high voltage output), high σ (to have low Joule heating), and low κ (to have large temperature difference) are necessary to realize high ZT_{avg} materials [7]. Unfortunately, due to the inter-dependence of these parameters, nature does not provide any single material with these favorable properties. Therefore, any approach based on the decoupling or balancing of these three parameters (i.e. α, σ and κ) for synergetic optimization of electrical and thermal transport is highly desirable for designing the material with high ZT_{avg} [7]. Apart from the need of p- and n-type materials with high ZT_{avg}, the choice of interconnect materials, buffer layer between interconnect and thermoelements play very important roles in extracting the maximum output power from TEG [8]. In summary the development of an efficient TEG from individual thermoelectric p- and n-type thermoelements is a big challenge and requires following three major key issues to be addressed [9]:

(i) Requirement of p- and n-type thermoelements with high average figure-of-merit (ZT_{avg}) in the temperature zone of application.
(ii) Joining of p- and n-type thermoelements with metallic interconnect having very low specific contact resistance (ρ_c) at metal/thermoelement interface.
(iii) Maximum heat transfers thorough the thermoelements while minimizing the thermal shunt path between hot surface and cold end.

2.1. Thermoelements with high ZT

In order to have highly efficient TEG, one of the most important requirements is that materials of both p- and n-type thermoelements should have high ZT_{avg} of nearly similar value at the operating temperature. The maximum theoretical efficiency expected for TEG as a function of temperature difference between hot and cold ends (assuming the cold end is at 300 K) for materials having different ZT_{avg} is shown in Fig. 2. Theoretically, for a material of $ZT_{avg} \sim 3$ a conversion efficiency (~30% at ΔT of 500 K) can be achieved, which is comparable to the conventional mechanical generators [10]. However, on the experimental side the situation for high ZT materials is quite different. The temperature dependence of ZT for various n- and p-type thermoelectric materials is shown in Fig. 3 [11]. It is seen that the highest ZT of most of the materials lies in the range of 0.8–1.2. Depending upon the peak ZT, conventional thermoelectric materials can be characterized based on their operating temperature range [1,2]:

(i) Materials for low temperature range (<250 °C), which includes Bi_2Te_3, Sb_2Te_3,
(ii) Materials for mid temperature range (250–650 °C), which includes PbTe and TAGS-85, and
(iii) Materials for high temperature range (>650 °C), which includes SiGe alloys.

From Fig. 3, it can also be seen that in last few years' various new materials, such as, PbTe–SrTe and skutterudites (for mid temperature), $Yb_{14}Mn_{1-x}Al_xSb_{11}$, $La_{3-x}Te_4$ (for high temperature) with high ZT have been investigated. Conventionally the peak ZT is used to evaluate the usability of the thermoelectric materials; however peak ZT does not guarantee high efficiency. For obtaining high efficiency of a TEG, the average ZT over the working temperature range is a more important parameter.

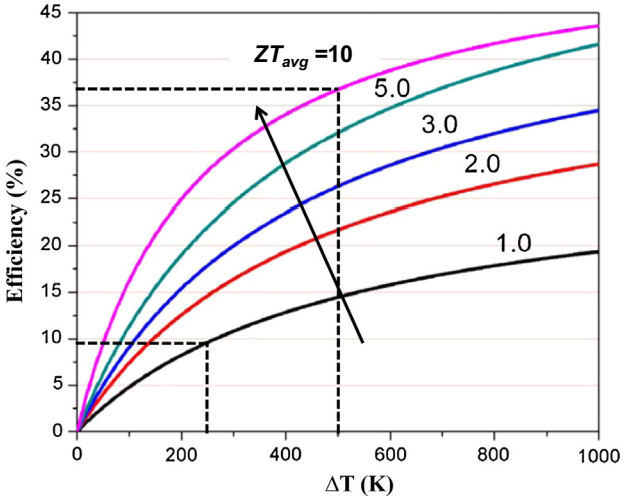

Fig. 2. Theoretical maximum efficiency of TEG as a function of temperature difference ΔT (cold source is at 27 °C). Reprinted with permission from Chen et al. [10]. Copyright 2012 Elsevier Ltd.

According to Eq. (1) in order to achieve high efficiency, it is essential that TEG are fabricated using high ZT materials with a large temperature gradient. Since ZT vary with temperature, it is not possible to use the same material throughout the entire large temperature gradient. One way to circumvent this problem is to use different materials that can be segmented together in such a way that a material with high ZT at high temperature is segmented with a different material with high ZT at low temperature. In this way, both materials operate in their most efficient temperature ranges. However, when two materials are being segmented for large temperature gradient applications, they must be thermoelectrically compatible with each other. The requirement of thermoelectric compatibility comes from the fact that to maintain maximum efficiency same heat and electric charge must flow through the material connected electrically in series. The thermoelectric compatibility factor for a particular material can be expressed as $s = [(1 + ZT)^{1/2} - 1]/\alpha T$ [12,13]. If the compatibility factor for two materials differ by more than about a factor of 2, not all the segments will perform with the best efficiencies, and as a result, the overall efficiency of the TEG will be substantially less than that predicted from the individual material's average ZT. The compatibility factor(s) for various p- and n-type materials are shown in Fig. 4.

From the compatibility factor data shown for p-type materials, it can be seen that SnTe and TAGS-85 has close compatibility factor around 500 °C, hence these materials has been successfully used for making segmented legs in mid temperature range operating TEG on several NASA space mission [1]. Similarly, a nearly matching compatibility factor of skutterudite $CeFe_4Sb_{12}$ and TAGS-85 may yield high efficiency on segmentation [12]. The closeness of compatibility factor for n-type PbTe with $CoSb_3$ may yield high efficiency on segmentation [12]. It is therefore evident from Fig. 4, that in order to obtain high efficiency, materials exhibiting high ZT in different temperature range should be judiciously chosen for segmentation.

In recent years, significant efforts have been made to design and synthesize new thermoelectric materials with enhanced ZT.

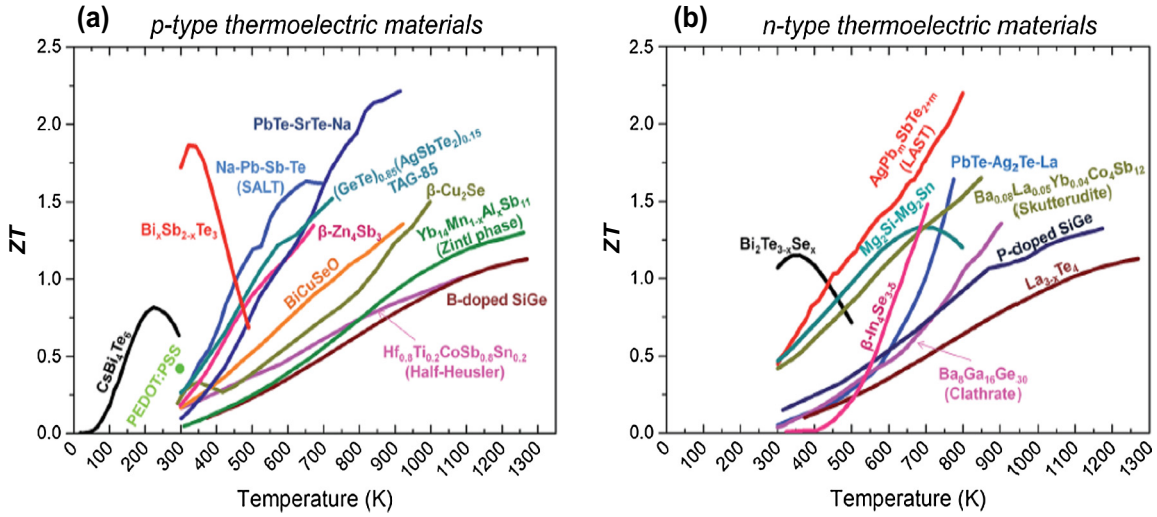

Fig. 3. Summary of the temperature dependence of *ZT* of thermoelectric n- and p-type materials. Reprinted with permission from Rull-Bravo et al. [11].

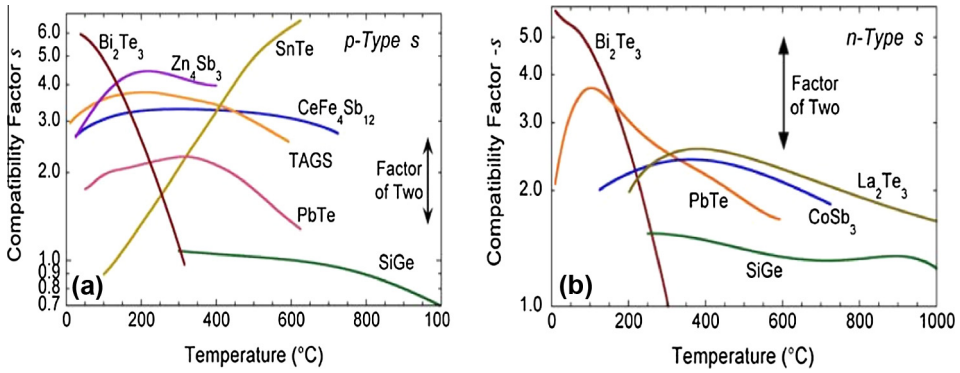

Fig. 4. Compatibility factor (s) for various (a) p- type and (b) n-type materials. Reprinted with permission from Snyder et. al. [12].

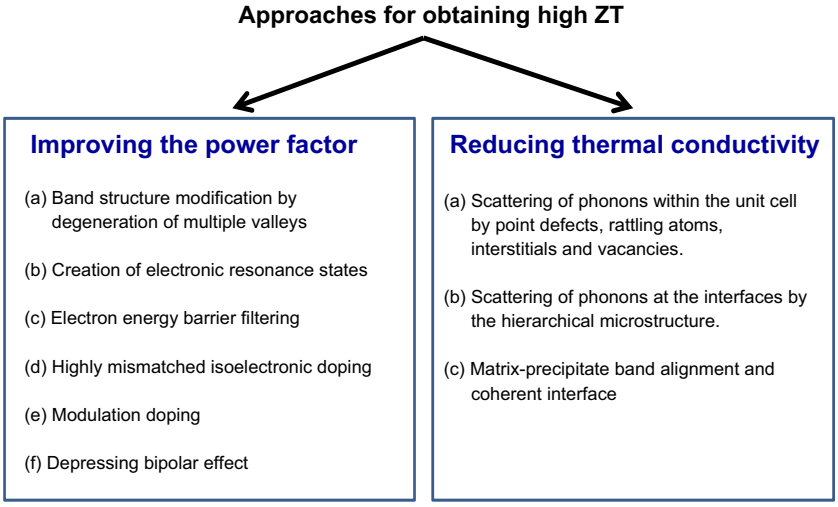

Fig. 5. Different strategies used to enhance the figure-of-merit (*ZT*) of various material either by enhancing the power factor ($\alpha^2\sigma$) and/or reducing the thermal conductivity (κ).

Various approaches adopted for enhancing the *ZT* can be either enhancement of power factor ($\alpha^2\sigma$) and/or reduction κ, as summarized in Fig. 5. A brief overview of these approaches is discusses below.

2.1.1. Enhancing the ZT through power factor ($\alpha^2\sigma$) enhancement

Various mechanisms that have been adopted for enhancing the power factor, $\alpha^2\sigma$, are schematically represented in Fig. 6, which are briefly discussed below.

(a) Modifying band structure by degeneration of multiple valleys

Under parabolic band and energy-independent scattering approximation α is defined as [7]:

$$\alpha = \frac{8\pi^2 m^* k_B^2 T}{3eh^2}\left(\frac{\pi}{3n}\right)^{2/3} \quad (3)$$

Here n is the carrier concentration and m^* is the density of states effective mass of the carrier. As evident from Eq. (3), the α at a given n can be enhanced by increasing the m^*. The m^* is given by the expression: $m^* = N_V^{2/3} m_b^*$ where $m_b^* \sim 1/(d^2E/dk^2)$ is the band effective mass and N_V is the number of conduction bands. Thus, m^* can be enhanced either by a material having flat bands (i.e. high m_b^*) or by increasing the N_V (e.g. materials having multiple valleys). The ZT of the materials can be improved through enhancement of m^* only if the charge carrier mobility is not affected and this can be achieved for materials having bands with multiple valleys [14,15]. Thus in case of n-type materials to enhance the N_V, multiple band valleys should be in conduction band, while for p-type materials it should be in the valence band.

The experimental evidence of the band structure modification has been demonstrated in n-type PbTe samples doped with either I on the Te site or La on the Pb site [15], which was carried out in such a manner that the carrier concentration remains unchanged (i.e. 1.8×10^{19} cm^{-3}). It has been shown that m^* in La doping is ~20% higher than that in I doping (near the optimal doping level) in the whole temperature range. The value of N_V was 4 in both the cases. The net effect of increased m^* is to increase α in La doped sample. However, the overall ZT of La doped sample was found to be lower than the I doped samples, mainly due to the reduction in the charge carrier mobility.

(b) Electronic resonance states

As represented by Eq. (3), α is related to m^*, which can be increased if the density of states (DOS) at E_F can be enhanced significantly. The DOS at E_F can be enhanced by doping the thermoelectric materials in such a way that the energy level of the dopant lies in the vicinity of the E_F of the thermoelectric material [16]. The distortion due to resonance in the energy levels enhances DOS at the E_F. In general, the sharper the local increase in DOS, the larger the enhancement in m^* and in α. The experimental evidence of modification of density states by dopants has been demonstrated for thallium doped PbTe samples ($Tl_{0.02}Pb_{0.98}Te$) [16]. It has been found that doping with Tl enhances the α of PbTe by a factor between 1.7 and 3 in the whole temperature range. However, the ZT value of such doped samples at 773 K was found to be 1.5, which is quite high as compared to the undoped sample.

(c) Electron energy barrier filtering

In the energy-filtering approach, the energy barriers are employed to block the low-energy electrons, and therefore, increases the average heat transported per carrier by the high energy electrons (resulting in high α) [9]. Such effects have been observed in the thermoelectric multilayers. In case of bulk materials, the nanostructured grains are often included in the matrix of thermoelectric materials so that the interfaces act as effective energy filters. However, it is likely that these interfaces may also substantially reduce the carrier mobility. Thus, energy filtering approach requires a careful design of the nanostructures so that optimum power factor is obtained. For example, Dy doped TAGS-85 shows enhancement of α due to an energy filtering mechanism. The potential barrier in this case has been created due to the mismatched atomic sizes and large magnetic moment of the Dy atoms present in the lattice [17]. The energy filtering effect has also been

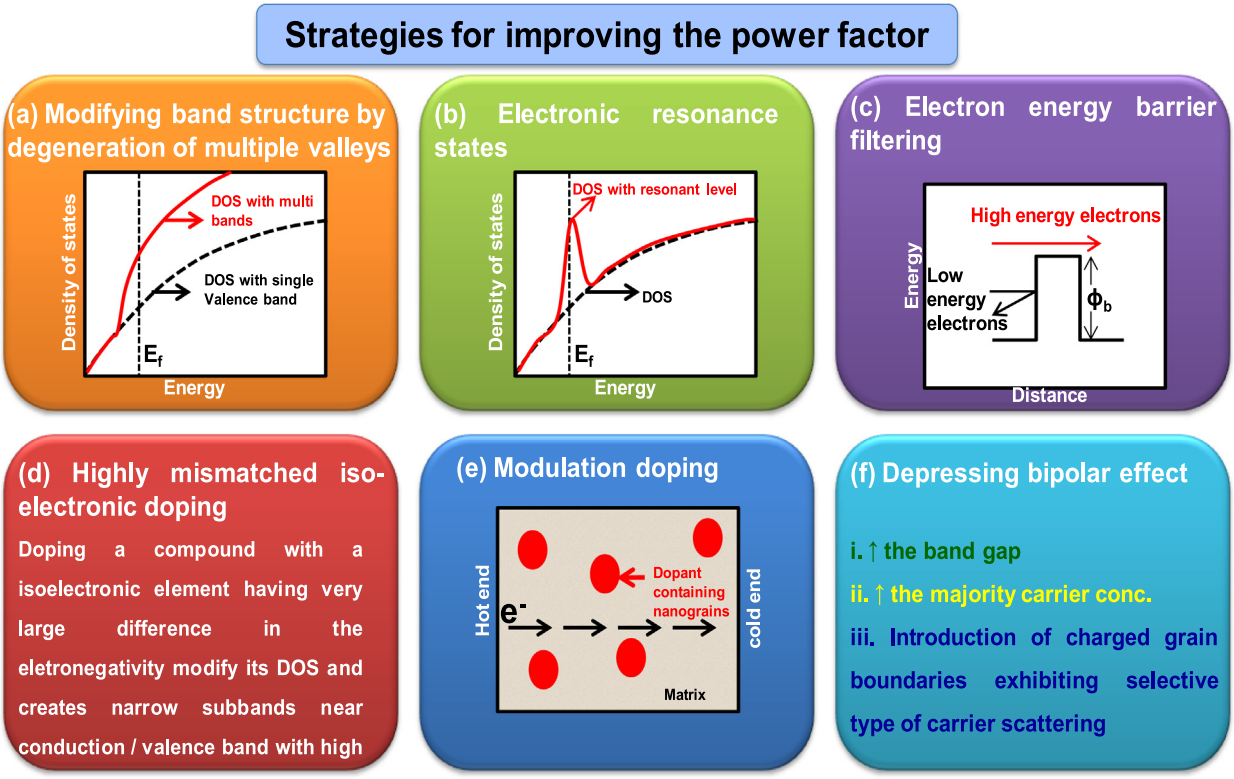

Fig. 6. Strategies employed for improving the power factor of various thermoelectric materials.

demonstrated at the organic–inorganic semiconductor interface of poly(3-hexylthiophene) (P3HT) and Bi_2Te_3 nanowires as the composite exhibited enhancement of power factor by nearly 3.5 times as compared to that of pure P3HT [18].

(d) Highly mismatched isoelectronic doping

High mismatched alloys (HMA) are a kind of semiconductors containing isoelectronic elements with very large differences in terms of atom size, ionicity, and electronegativity, and therefore exhibit unusual and fundamentally different electronic/optical properties [19]. The synthesis of HMA involves alloying of isovalent but highly electronegative mismatched constituents at dilute concentrations. However, due to large miscibility gaps, synthesis of HMA is usually difficult. In HMAs, the hybridization between the extended states of the majority component and the localized states of the minority component results in a strong band restructuring, leading to peaks in the DOS and creation of new sub-bands near the original conduction or valence band edge. These narrow sub-bands formed in HMAs have a heavy effective carrier mass due to their localized origin and give rise to a sharp DOS distinct from those of the host material, which are responsible for high α. In order to explain this strategy, Lee et al. have investigated the effect of O impurities on the thermoelectric properties of ZnSe. It has been demonstrated that dilute amounts of O impurities introduce peaks in the density of states (DOS) above the conduction band minimum and the charge density near the DOS peaks is substantially attracted toward O atoms due to their high electronegativity. The impurity-induced peaks in the DOS resulted in a sharp increase in the room-temperature value of α, and hence, power factor respectively by a factor of 30 and 180 as compared to those of O free ZnSe [19].

(e) Modulation doping

In modulation doping approach the free electrons in the matrix of thermoelectric materials are spatially separated from the possible donor ions so that their scattering by the dopant atoms is avoided and hence their mobility remains high [20,21]. As a consequence, the conductivity of materials remains high leading to improved power factor. Modulation doped samples are usually two phase nanocomposites made out of two different types of nanograins. Rather than uniformly doping the sample, the dopants are incorporated into only one type of nanograins. Charge carriers will spill over from the doped nanograins to the undoped or lightly doped matrix phase, leaving behind ionized nanograins. Thus the electrical conductivity of the two-phase composite can exceed that of the individual components, leading to a higher power factor. The experimental evidence for modulation doping has been demonstrated for $Si_{95}Ge_5$ alloys (i.e. matrix) where heavily doped $Si_{70}Ge_{30}P_3$ nanograin acts like a charge reservoir. In this study it has been shown that the conduction band edge of the nanograin is higher as compared to that of matrix grains facilitating easy transfer of electrons from nanoparticles to matrix. Such sample exhibit an increase in the mobility, as the ionized impurity is confined to the nanograin. The enhanced mobility increases the power factor by 20%. On the other hand, incorporation of $Si_{70}Ge_{30}P_3$ increases the thermal conductivity. However, the increase in power factor compensates for the increase in thermal conductivity and as a result the *ZT* improves by 10% [20]. Power factor of the p-type $Si_{86}Ge_{14}B_{1.5}$ uniform sample was improved by 40% using the modulation-doping approach [21].

(f) Depressing bipolar effect

Thermoelectric materials are in general narrow band gap semiconductors and thus have mixed carriers (electrons and holes) in each band, especially at high temperature, i.e. electrons in the valence band can partially hop to the conduction band and vice versa. This diffusion creates electron–hole pairs: the so-called bipolar effect. Bipolar effect has the disadvantage because the minority charge carriers get thermally excited across the band gap and thus decreases the overall α [22]. Following three ways depress the bipolar effect: (i) increasing the majority charge carrier concentration which shifts the Fermi level and may decrease the onset of minority carrier effect by increasing the energy required to do so; (ii) increasing the band gap, which delays the onset of thermally activated minority carriers at high temperature; (iii) synthesis of mesoscale microstructures with grain boundaries. These grain boundaries act as an interface which produces interfacial potential and thus scatter electron and holes differentially, thereby deteriorating the bipolar effect. The role of suppression of bipolar thermal conductivity in enhancing the *ZT* has been demonstrated for PbTe alloyed with a wider band gap compound, such as, MgTe. Since MgTe has a good solubility in PbTe, therefore PbTe–6%MgTe alloyed samples exhibited higher band gap, and therefore, an enhancement of *ZT* ($\sim$2 at 900 K, pure PbTe the $ZT \sim 1.1$ at 900 K) has been observed [23].

2.1.2. Enhancing the ZT via reduction in thermal conductivity

In addition to improving power factor ($\alpha^2\sigma$), as discussed above, the *ZT* can be enhanced by reducing the total thermal conductivity (κ) in such a way that the electrical conductivity is not reduced. The κ of a material is given by [23]:

$$\kappa_{tot} = \kappa_e + \kappa_{bi} + \kappa_l \quad (4)$$

where κ_e, κ_{bi}, and κ_l are electronic, bipolar and lattice contributions, respectively. κ_e is directly related to the σ through Wiedemann–Franz law as [24]:

$$\kappa_e = L\sigma T \quad (5)$$

where L is Lorentz number and it is $2.4 \times 10^{-8}\ J^2\ K^{-2}\ C^{-2}$ for free electrons. The linear dependence of σ and κ_e according to Wiedemann–Franz law suggest that effective way to maximize the *ZT* is to tailor the $\kappa_{bi} + \kappa_l$. Usually, the contributions from κ_e and κ_{bi} are much smaller than that of κ_l. However, κ_{bi} becomes dominant only at high temperatures. The κ_l is dominating as phonons of different wavelengths contribute to the heat conduction, and therefore, in literature various approaches have been adopted to reduce κ_l, which can be broadly classified into following two categories.

(a) Scattering of phonons within the unit cell

In this case phonons are scattered within the unit cell by creating rattling structures or point defects, such as, interstitials, vacancies or by alloying [1,2]. Use of complex crystal structures result in high electronic conductivity due to periodic crystal structure, while low thermal conductivity is obtained by rattling of phonons [7]. This is a popularly known as phonon glass and electron crystal (PGEC) approach that was proposed by Slack [1,25].

(b) Scattering of phonons at various interfaces of nanometer scales

In a material, phonons that transport heat have wide spectrum of wavelengths and mean free paths, and each of them contribute to the lattice thermal conductivity. The short and medium mean free path phonons are strongly scattered by the point defects and the nanostructures, respectively. The scattering of long mean free path phonons is mainly achieved by introducing the structures (having sizes 100 nm–5 μm) in the matrix. Therefore, in order to minimize the thermal conductivity, it is essential that phonons of all mean free paths are scattered, which can be achieved by introducing all length scale hierarchical architectures in the matrix, as schematically shown in Fig. 7(a) [6,26]. In other words, solid

solution point defects, nanostructures, grain boundaries, mesoscale structures all must be integrated in a single sample. In a recent report, the contribution of phonon scattering in PbTe and Si samples having all length scale hierarchical architectures has been estimated and the result is shown in Fig. 7(b). From there it can be seen that for both materials, around 25% of κ_l is contributed by the phonon modes with mean free path less than 5 nm and around 55% of κ_l is contributed by the phonon modes with mean free path between 5 and 100 nm. The remaining 20% of κ_l is contributed by the phonon modes with mean free path of 0.1–1 μm.

(c) Matrix-nano precipitate band alignment and coherent interface

It is important to mention here that though the strategy of creating all length scale hierarchical architecture in materials can dramatically reduce thermal conductivity, however it can also reduce the power factor due to lowering of charge carrier mobility. Thus the ideal situation for improving *ZT* is to reduce thermal conductivity without affecting the charge carrier mobility [6]. In principle, this can be achieved by introducing appropriate secondary phases in the bulk matrix that has the following characteristics: (i) secondary phase forms coherent interfaces with matrix i.e. there is a lattice matching; and (ii) the conduction/valance bands of matrix and precipitate should match in energies for facile electron/hole transport. Such a scheme is schematically shown in Fig. 8, which allows the charge transport but scatters the phonons. The experimental demonstration of matrix–precipitate band alignment with coherent interface has been demonstrated for p-type PbTe matrix with SrTe nanocrystals as precipitates. In this system strong reduction of κ_l without affecting power factor resulted in very high *ZT* of ~2.2 at 642 °C [6,26].

Table 1 provides a brief summary of literature on the *ZT* values for various thermoelectric materials according to their temperature range of operation. It is seen that for low temperature thermoelectric applications (<250 °C) inorganic semiconductor alloys, such as, bismuth tellurides exhibit high *ZT*. However, they exhibit high density and brittleness and therefore pose limitations for commercial applications where mass and flexibility of the devices is main concern. Therefore, in this context organic thermoelectric material have advantages as they are environment friendly, lightweight, tunable properties by molecular chemistry and doping

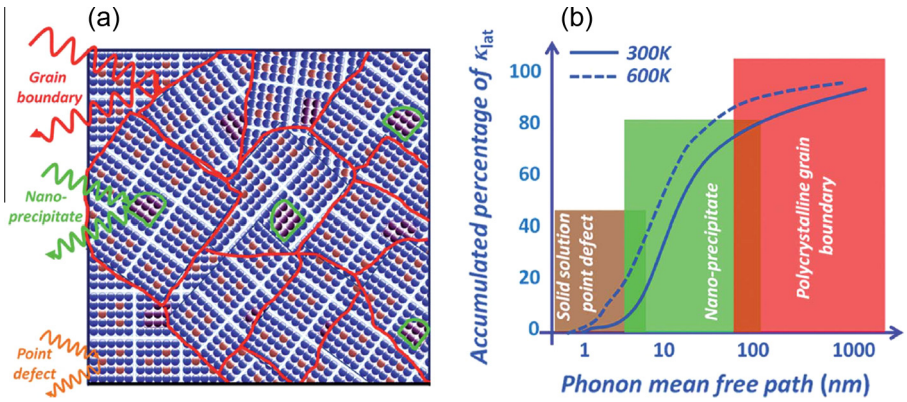

Fig. 7. (a) All-scale hierarchical architectures exhibiting the scattering of phonons of different mean free paths and (b) cumulative distribution function of lattice thermal conductivity with respect to the phonon mean free path in Si or PbTe bulk. Reprinted with permission from Zhao et al. [6].

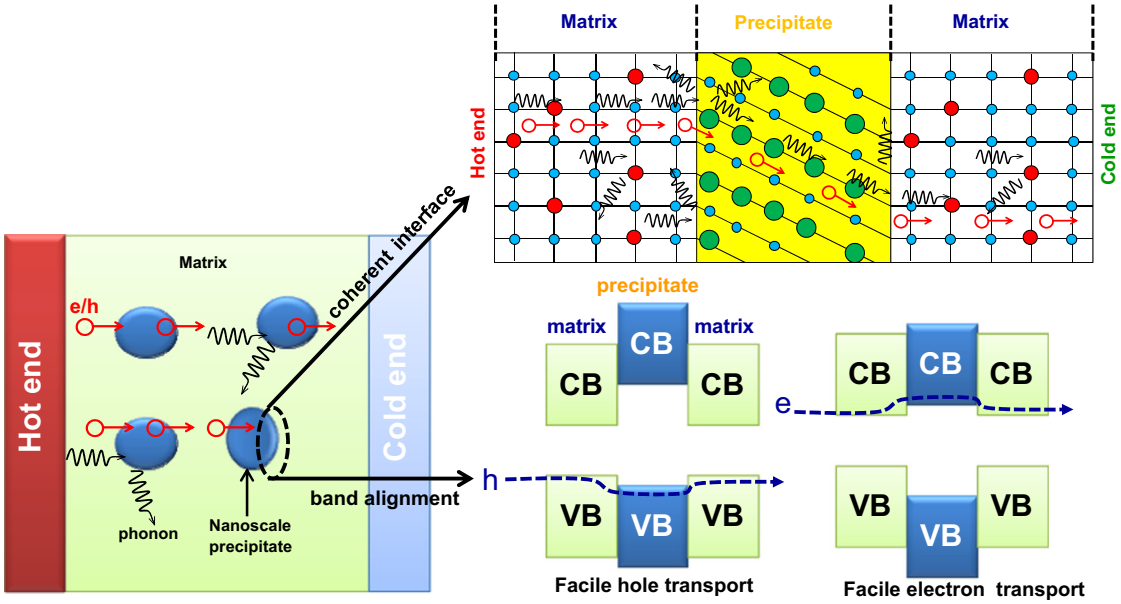

Fig. 8. Schematic showing the facile electron/hole transport through a coherent interface between matrix and precipitate that also scatters heat carrying phonons. Relative energy band diagram for the combined matrix and precipitate showing the large differences in semiconducting band gap and the small energy difference between valence/conduction bands is required for facile hole/electron transports.

Table 1
Brief summary of *ZT* for various thermoelectric materials.

Temperature range	Materials		Type	*ZT*	Ref.
<25 °C	$CsBi_4Te_6$		p-type	0.8 at −48 °C	[27]
	Sn doped BiSb alloy		p-type	0.13 at −35 °C	[28]
	$Bi_{85}Sb_{14}Pb_3$			0.11 at −123 °C	[29]
25–250 °C	$Bi_2Te_{3-x}Se_x$		n-type	1.15 at 97 °C	[30]
	$Bi_{0.5}Sb_{1.5}Te_3$		p-type	1.86 at 47 °C	[31]
	Poly(3,4-ethylenedioxythiophene) [PEDOT]		p-type	0.25 at 23 °C	[32]
	n-type poly[Nax(Ni-ett)]		n-type	0.15 at 127 °C	[33]
	p-type poly[Cux(Cu-ett)]		p-type	0.01 at 127 °C	[33]
	Poly(styrenesulphonate) in poly(3,4-ethylenedioxythiophene) PEDOT:PSS		p-type	0.42 at 27 °C	[34]
	$Cu_2Se_{1-x}I_x$		p-type	2.3 at 27 °C	[35]
250–650 °C		PbTe–SrTe alloys	p-type	2.2 at 642 °C	[26]
	Tellurides	MgTe–PbTe	p-type	2.0 at 550 °C	[23]
		$AgSbTe_2$–$AgSbSe_2$	n-type	0.65 at 247 °C	[36]
		$AgPb_mSbTe_{2+m}$ (m = 18)	n-type	2.2 at 527 °C	[37]
		$(AgSbTe_2)_{0.15}(GeTe)_{0.85}$ i.e.TAGS-85	p-type	1.5 at 427 °C	[1]
	Silicides	$Mg_2Si_{0.4}Sn_{0.6}$	n-type	1.1 at 527 °C	[38]
		$Mg_2Si_{0.85}Bi_{0.15}$	n-type	0.67 at 500 °C	[39]
		$Mg_2Si_{0.53}Sn_{0.4}Ge_{0.05}Bi_{0.02}$	n-type	1.4 at 527 °C	[40]
		$MnSi_{1.73}$	p-type	0.47 at 600 °C	[41]
		$MnSi_{1.75}$	p-type	0.63 at 450 °C	[42]
	Antimonides	β-Zn_4Sb_3 based alloys	p-type	0.8 at 277 °C	[38]
	Selenides	$CuCrSe_2$	p-type	1 at 500 °C	[43]
		$AgCrSe_2$	p-type	1 at 500 °C	[44]
		$(CuCrSe_2)_{0.5}(AgCrSe)_{0.5}$	p-type	1.4 at 500 °C	[45]
		PbSe based alloys; PbSe–CdS	p-type	1.6 at 650 °C	[46]
		SnSe single crystal	p-type	2.6 at 650 °C	[47]
	Skutterudites	$Ba_{0.08}La_{0.05}Yb_{0.04}Co_4Sb_{12}$	n-type	1.7 at 577 °C	[48]
		$CoSb_{2.75}Sn_{0.05}Te_{0.2}$	n-type	1.1 at 550 °C	[49]
		$Co_4Sb_{11.4}Te_{0.6}$	n-type	0.95 at 527 °C	[50]
		$CoSb_{2.75}Ge_{0.05}Te_{0.2}$	n-type	1.1 at 527 °C	[51]
		$Co_{3.9}Ni_{0.1}Sb_{11.5}Te_{0.4}Se_{0.1}$	n-type	1.1 at 452 °C	[52]
		$CoFe_{4-x}Co_xSb_{12}$	p-type	1.4 at 627 °C	[53]
		$Co_{0.28}Fe_{1.5}Co_{2.5}Sb_{12}$	p-type	1.1 at 477 °C	[54]
		$Yb_{0.25}La_{0.6}Fe_{2.7}Co_{1.3}Sb_{12}$	p-type	0.99 at 427 °C	[55]
		$DD_{0.7}Fe_{2.7}Co_{1.3}Sb_{11.8}Sn_{0.2}$ (DD stands for didymium filler i.e. 4.76%Pr and 95.24% Nd)	p-type	1.3 at 507 °C	[56]
	Quarternary chalcogenides	$Cu_{2.1}Cd_{0.9}SnSe_4$	p-type	0.65 at 450 °C	[57]
		$Cu_{2.1}Zn_{0.9}SnSe_4$	p-type	0.9 at 587 °C	[58]
		$Cu_2ZnSn_{0.9}In_{0.1}Se_4$	p-type	0.95 at 577 °C	[59]
	Half Heuslers	$Hf_{0.5}Ti_{0.25}Zr_{0.25}NiSn_{0.99}Sb_{0.01}$	n-type	1 at 500 °C	[60]
		$Ti_{0.25}Zr_{0.75}NiSn_{0.975}Ge_{0.025}$	n-type	0.48 at 502 °C	[61]
		$Ti_{0.5}Hf_{0.5}CoSb_{0.9}Sn_{0.1}$	p-type	0.3 at 502 °C	[64]
	Sulphide	PbS-CdS	p-type	1.3 at 650 °C	[65]
>650 °C		$Si_{80}Ge_{20}$ alloys	n-type	1.8 at 800 °C	[66]
			p-type	1.2 at 800 °C	[67]
		$Si_{80}Ge_{18}B_2$	n-type	0.67 at 727 °C	[68]
		Zintl compound: $Yb_{14}MnSb_{11}$	p-type	0.8-1.0 at 927 °C	[69]
		Yb substituted $La_{3-x}Te_4$	n-type	1.1-1.2 at 1002 °C	[70]
		$Nb_{0.6}Ti_{0.4}FeSb_{0.95}Sn_{0.05}$	p-type	1 at 700 °C	[63]
		$Bi_{0.875}Ba_{0.125}CuSeO$	p-type	1.4 at 650 °C	[71]
		$CuSe_{2-x}$	p-type	1.5 at 727 °C	[72]
		Cu_2Se	p-type	2.1 at 700 °C	[73]
	Half Heuslers	$FeNb_{0.8}Ti_{0.2}Sb$	p-type	1.1 at 827 °C	[59]
		$Nb_{0.6}Ti_{0.4}FeSb_{0.95}Sn_{0.05}$	p-type	1 at 800 °C	[60]
		$Hf_{0.44}Zr_{0.44}Ti_{0.12}CoSb_{0.8}Sn_{0.2}$	p-type	1 at 800 °C	[62]
		$FeNb_{0.88}Hf_{0.12}Sb$	p-type	1.5 at 927 °C	[63]

treatments, flexibility and low-cost fabrication using solution-processing methods. However, the highest reported *ZT* value for organic thermoelectric materials is significantly lower than the inorganic thermoelectric materials. It is expected that with growing worldwide interest in organic thermoelectric materials, their *ZT* would improve in coming years [31,36]. For low, mid and high temperature ranges, several inorganic n- and p-type thermoelectric materials with *ZT* approaching to 2 are available. In order to fabricate the TEG, the selection criteria for choosing the n- and p-type thermoelectric materials are as follows:

(i) The first and foremost important criteria is that materials should exhibit high and stable average *ZT* over a wide range of temperatures for several years. Thermal stability of *ZT* is decided by the stability of α, σ and κ. The root cause of degradation of thermoelectric properties during prolonged

operation are usually formation of voids or cracks, sublimation of the material, reaction of materials with atmospheric gases and/or with metallic interconnects. Therefore, the thermoelectric material should be chemically and mechanically stable at high temperatures.

(ii) The thermoelectric materials should be machinable so that they can easily be sliced or polished into optimized shape and size.

(iii) From commercial application point of view, the material should be available in abundance at economic price and can be synthesized using facile and scalable processes.

As seen from Table 1, various thermoelectric materials essentially fall into the categories of chalcogenides, skutterdites, half-Heuslers, silicides and oxides. Chalcogenides (e.g. Bi_2Te_3, Bi_2Se_3, PbTe, PbSe, SnTe, SnSe, $AgCrSe_2$, $CuCrSe_2$, $TiSe_2$, $AgSbTe_2$, TAGS-85, PbS, etc.) have shown potential for low and mid temperature range applications. Since tellurium is relatively costly due less abundance in earth, therefore in most of the chalcogenides compounds for employed for commercial TEGs, it is being replaced by Se. Skutterdites (MX_3 family, where M is the transition metal element Co, Rh, Ir and X is pnictogen element such as P, As, or Sb) are quite promising low cost materials for mid temperature range TEGs. Skutterdites compound are known for their high electron mobility and reasonably high Seebeck coefficient but they have high lattice thermal conductivity. In skutterdites filling the voids in the structure by the elements (which are also n-type dopant) that are loosely bound, result in the lowering of lattice thermal conductivity. Half-Heusler (HH) compounds have the elemental formula *XYZ*, where *X*, *Y* and *Z* can be selected from many different elemental groups (for ex. *X* = Ti, Zr, Hf, V, Mn or Nb; *Y* = Fe, Co, Ni or Pt; *Z* = Sn or Sb. These materials exhibit impressive thermoelectric properties at mid and high temperature range. The crystal structure of these compound consist of three intercalated face centered cubic (fcc) sublattices and exhibit low band gap of magnitude in the range of 0.2–2 eV. The most attractive properties of HH materials are high Seebeck coefficient (up to 300 μV/K at room temperature) along with high electrical conductivity (~1000–10,000 S cm^{-1}). HH materials exhibit high thermal conductivity (~10 W/mK). The HH compound has the advantage to optimize their thermoelectric properties by doping each of the three occupied *fcc* sublattices. For example, it is possible to enhance the carrier concentration by doping in the *Z* position and simultaneously introducing disorder by doping on the *X* and *Y* position resulting in mass fluctuations for decreasing lattice thermal conductivity. At present lots of research is going on HH compounds and these materials have a strong potential for commercial application due to their environment friendly nature, low cost, easy availability of the raw materials, easy processing conditions for large scale production and high chemical and mechanical resistance at high temperatures. However, the long term stability of the HH compounds needs to thoroughly investigated at high temperatures. Silicides are the compound that contains silicon. Although silicon is not a good thermoelectric material due to its high thermal conductivity but it is one of the most desirable semiconductor for any application due to its huge abundance in the earth. Alloying a small amount of germanium with silicon creates point defect that scatters phonons and such an alloy exhibit low thermal conductivity and high $ZT \sim 1$ at 900 °C. With nanostructuring approach, $ZT \gg 1$ has been achieved for both n- and p-type $Si_{80}Ge_{20}$ alloys. SiGe alloys are one of the proven materials used in various space missions by NASA. If Ge can be replaced by another low cost material, then such Si based materials would be very attractive for commercial applications. In fact, nanostructured bulk silicon exhibits *ZT* of 0.7 at 930 °C, and therefore, are potential candidate for future applications. Among silicon based alloys, higher manganese silicide (HMS) alloys are p-type while magnesium silicides are n-type, making them suitable for development of TEGs in the mid temperature range.

2.2. Joining of p- and n-type thermoelements with metallic interconnects

As shown in Fig. 1, the electrical resistance of the TEG depends not only on the electrical resistance of the thermoelectric legs that consist of p- and n-type thermoelements but also the electrical resistance of the metal interconnects and the contact resistance between interconnects and thermoelements. All of these resistances are temperature dependent, and therefore, exact computation of the TEG resistance as a function of temperature is very complex. However, assuming temperature independence, the device resistance, *R*, can be approximated as:

$$R = n\left[\frac{\rho_n^l}{A_n} + \frac{\rho_p^l}{A_p} + R_c\right] \tag{6}$$

where ρ_p and ρ_n is resistivity of p- and n-type thermoelements, R_c is a sum of interconnect and contact resistance of p- and n-type thermoelements, l is the length (height) and A is the cross-sectional area of the each thermoelements. According to Eq. (6), contact resistance can be estimated by subtraction of total material resistance (i.e. thermoelements and interconnects) from the resistance of TEG. Since worldwide different groups are using thermoelements of different dimension therefore for comparison it is appropriate to define the term specific contact resistivity ρ_c (Ω cm^2), which is defines as multiplication of contact resistance with the contact area. It is important to mention that ρ_c decreases the effective $(ZT)_{device}$ of the device in comparison to the $(ZT)_{thermoelement}$ of thermoelement according to relation [74]:

$$(ZT)_{device} = \frac{L}{(L + 2\rho_c\sigma)}(ZT)_{thermoelement} \tag{7}$$

Here L is the length of the thermoelement, σ is the electrical conductivity of the leg and $(ZT)_{thermoelement}$ is the average *ZT* of the thermoelement between hot end and cold end temperature. For a typical TEG, the $L \sim 5$ mm, $\sigma \sim 1000$ S cm^{-1}, ρ_c should be much less than $L/2\sigma \sim 2.5 \times 10^{-4}$ Ω cm^2. Ideally for an efficient TEG, the $\rho_c < 1$ μΩ cm^2 [8]. According to Eq. (7), if ρ_c is very high then the average *ZT* of TEG decreases, which in turn reduces the efficiency due to (i) the lowering of current generated by the thermoelectric material and (ii) the rise in temperature at contacts due to Joule heating will disturb the temperature gradient, leading to a decrease in α. Making good electrical contacts in TEG is challenging as the TEG operates under a large temperature difference, which leads to thermo-mechanical stress, diffusion and chemical reaction between thermoelectric material and interconnects. Ideal interconnect materials should have the following properties [8,9]:

(i) Its electrical and thermal conductivities should be higher as compared to the thermoelectric material.

(ii) It thermal expansion coefficient should match with that of thermoelectric material.

(iii) It should be prepared in very thin disc to reduce total electrical and thermal resistances.

(iv) It should exhibit low contact resistance at the interface between the contact material layer and thermoelectric layer.

(v) It should remain chemically stable and do not interact with the thermoelectric materials over the life time of the TEG.

(vi) It should have form strong diffusion bonds with the thermoelectric layer so that the contact remains mechanically strong.

The various interconnects as well as buffer layers used in fabrication of TEGs suitable for different temperature are discussed in a later section.

2.3. Minimization of thermal shunt path

As seen from Fig. 1, the heat can flow through the thermoelements as well as through the dead space between and surrounding the thermoelements through convective or radiative processes. In order to utilize maximum heat available at the source, not only the good heat exchanges at hot and cold ends are needed but one also needs to ensure an efficient flow of heat through the thermoelements. Similar to the electrical resistance, the total thermal conductance of a TEG can be approximated by:

$$\kappa = n\left[\frac{\kappa_n A_n}{l} + \frac{\kappa_p A_p}{l} + \kappa_s\right] \quad (8)$$

where κ_n and κ_p are respective thermal conductivity or n and p-type legs. A_n and A_p are respective cross-sectional area of n and p-type thermoelements. κ_s is the parallel thermal loss per couple. In order to minimize the thermal shunt path (κ_s), it is essential to fill the dead space between p and n-type thermoelements in the TEG with a highly thermally insulating material having thermal conductivity much lower than that of thermoelectric legs. This not only prevents the flow of heat through the dead space between thermoelements but also reduces the sublimation loss of high vapor pressure element from the thermoelements. In addition, the material used for thermal shunt path can provide mechanical support for the TEG.

3. Current status on the development of TEGs

Though many companies, such as, Yamaha Corporation (Japan), Gentherm Inc. (U.S.), II–VI Incorporated (U.S.), Ferrotec Corporation (Japan), Laird Plc. (U.K.), and Komatsu Limited (Japan) have already been marketing TEGs for various applications, the detailed know-how of the technologies for the fabrication of TEGs is not available in the literature. As discussed earlier, the major bottleneck in manufacturing the TEGs comes from the appropriate selection of the metallic interconnect and the techniques to bind them to thermoelectric material. For low temperature TEGs, metallic interconnects are joined to p- and n-type thermoelements by direct soldering. However, in some cases direct soldering is not possible due to the poor adhesion of soldering material onto thermoelements and/or soldering material reacts with thermoelements at operating temperature. In order to avoid these issues, normally the end surfaces of thermoelements are metalized using nickel, which not only provides better sticking of soldering material but also acts like a diffusion barrier [57]. The metallization can be carried out using thermal evaporation, sputtering, chemical vapor deposition or electroplating. However, in the case of high temperature TEGs, soldering is not good option, and therefore, metallic interconnects are joined to thermoelements by diffusion bonding process, in which bonding is achieved by providing high temperature and high pressure at the joints. Here we discuss, literature reports on fabrication of metallic contacts for TEGs for low, mid and high temperature ranges.

3.1. TEG for low temperature range (<250 °C)

Table 2 provides the summary of various TEG reported for low temperature range (<250 °C) along with the materials used for buffer and metallic interconnects. As discussed before bismuth tellurides/selenides exhibit high *ZT* at low temperature range (100–250 °C), hence these materials have extensively been used for the fabrication of TEGs. For Bi_2Te_3 based TEG, Cu or Ag stripes are normally used to interconnect the thermoelements. In general, electroplated nickel layer of ~1 μm thickness is used at the ends of the thermoelements to which metallic strips are joined using soldering materials [57]. In a recent report, it has been demonstrated that Bi_2Te_3 thermoelements modified with an organic layer (i.e. self-assembled 3-mercaptopropyl-trimethoxysilane) provides a good covalent bonding between Ni layer and ends of thermoelements [63]. With this modification, both p and n-type thermoelements exhibited contact resistance (ρ_c) of ~1 μΩ cm^2 [75]. It is important to mention that vacuum hot pressing of Ni powder at the ends of p-type Bi_2Te_3 thermoelements result in low ρ_c. However the reaction of Ni with n-type results in a relatively higher ρ_c (~210 μm cm^2) [74]. To overcome this issue, a thick layer of $Bi_2Te_{2.7}Se_{0.3}$ doped with 1% SbI_3 has been introduced in between Ni and n-type $Bi_2Te_{2.7}Se_{0.3}$, which resulted in mechanically strong contacts with ρ_c of <1 μm cm^2 [76]. An efficiency up to 8.5% have been reported for TEGs based on $MgAg_{0.965}Ni_{0.005}Sb_{0.99}$ [79]. Apart from bismuth tellurides/selenides for low temperature TEGs, efforts has recently been made to develop organic materials based TEGs. However, the reports show that due to high resistivity of the organic materials, a very low current can be extracted from such devices [77].

3.2. TEG for mid temperature range (250–650 °C)

Table 3 provides a summary of various TEGs reported for mid temperature range (250–650 °C). In this temperature range most widely used state-of-art thermoelectric materials are n- type PbTe and p type $(AgSbTe_2)_{0.15}(GeTe)_{0.85}$ i.e. TAGS-85. The RTG based on these materials have widely been used in the Mars mission of NASA. PbTe is prepared as n-type by using excess Pb [79]. However, p-type PbTe is prepared by doping with alkali metal such as Na, which is a bit difficult process. In addition, the mechanical strength of p-type PbTe is poorer as compared to n-type PbTe. Therefore, the p-type PbTe is replaced by high ZT and mechanically strong TAGS-85. In a recent study Ag is proposed as a bonding layer for PbTe based TEGs [80]. The schematic representations for making n-type PbTe and p-type TAGS thermoelectric elements with buffer layers with low ρ_c are shown are shown in Fig. 9(a and b). Ag/Fe layer has widely been used as the contact metal for n-type PbTe. The coefficient of thermal expansion of PbTe is significantly different than Fe, which causes the stress at the Ag/Fe interface at high temperatures and hence degrades the performance of TEG. To overcome this a few μm thick PbTe/Fe mixture layer (50% PbTe + 50% Fe) is introduced between the Fe and PbTe layers. In the case of p-type TAGS-85 thermoelements, Ag/Fe/SnTe layer have been used for making contacts. SnTe layer is introduced in between the TAGS-85 and the Fe contact layers to prevent reaction between TAGS-85 and Fe. The average specific contact resistivity for such as TEG was found to be 7.6 μΩ cm^2 [81].

The schematic of a 2 p–n legs TEG fabricated using n-type PbTe and p-type TAGS thermoelements is shown in Fig. 9(c) in which silver stripes were used as interconnects. The hosing of the device was done using asbestos, which has much lower thermal conductivity as compared to the thermoelements, and therefore, reduced the direct flow of heat from hot end to cold end. Typical output power of such 2p–n legs device for a hot end temperature of 500 °C and $\Delta T \sim 400$ °C is shown in Fig. 9(d). The efficiency of such TEG was found to be ~6% [81].

Filled skutterudites exhibit better thermoelectric properties as compared to conventional tellurides for mid temperature range power generation, and hence, considerable efforts have been made in literature to develop TEGs. In the case of filled skutterudite, Nb layer has been found to be a good choice as interconnects with ρ_c of <5 μΩ cm^2 [82]. Some groups have used Ti foil as buffer layer to

Table 2
Summary of various reported data for low temperature range (<250 °C) operating TEGs.

Thermoelements type	T_h/T_c	Interconnect material	Buffer layers at the ends	Efficiency (%)	Comments	Ref.
p-type Bi_2Te_3	150 °C/24 °C		Nickel	5.8	Formation of contacts by soldering	[78]
$MgAg_{0.965}Ni_{0.005}Sb_{0.99}$	245 °C/20 °C	Silver	–	8.5	Formation of contacts by diffusion bonding	[79]
n-type poly[Nax(Ni-ett)] and p-type poly[Cu_x(Cu-ett)]	147 °C/67 °C	Silver at cold end and aluminum at hot end	Gold	–	Module resistance ~33 Ω, 35 n-p couples delivered an output voltage of 0.26 V, a current of 10.1 mA, and a power of 2.8 μW	[77]

join $CoSb_3$ and Mo–Cu or W–Cu alloy contact with an effective ρ_c of 20–30 μΩ cm^2. Fleurial et al. used Ti as metal contacts for both n- and p-type filled skutterudite, with a Zr layer in between as a diffusion barrier and in this study ρ_c is ~19 μΩ cm^2 [83]. An intermetallic compound layer also formed at the Zr/$CoSb_3$ interface after aging test. Guo et al. reported using arc-melted Co–Fe–Ni alloys as electrodes as well as diffusion barriers in filled skutterudite modules [84]. Muto et al. used $CoSi_2$ for the n-type and Co_2Si for the p-type electrodes for skutterudite and the ρ_c was found to be ~1–2 μΩ cm^2 [86]. A typical photograph of skutterudite based 32 couples TEG is shown in Fig. 10, which are reported to have an efficiency of >6%. In these devices, silica based aerogels were used to fill the dead space between thermoelements [87].

In the mid temperature range, n-type Mg_2Si is another interesting material that exhibits excellent thermoelectric properties. However, the counterpart p-type Mg_2Si exhibited poor thermoelectric properties. Therefore, reported TEG based on Mg_2Si are either a unileg structure consisting of only n-type Mg_2Si legs or contain other p-type materials, such as $NaCo_2O_4$. Ni is normally used as interconnect for n-type Mg_2Si as it does not react with Mg_2Si at the working temperature of 650 °C [88,89]. The bonding between Ni and Mg_2Si was achieved using direct hot-press method. However, ρ_c for such contacts was found to be ~100 μΩ cm^2. In the case of Sb-doped Mg_2Si which has very high electron concentration, the ρ_c was found to be ~32 μΩ cm^2 [88]. In a very recent report Ni was bonded to doped Mg_2Si using a current assisted sintering method and low ρ_c of ⩽10 μΩ cm^2 has been achieved [89].

3.3. TEG for high temperature range (>650 °C)

A summary of various reported data for TEG operating at high temperature range (>650 °C) is presented in Table 4. Iron disilicide (β-$FeSi_2$) was proposed for thermoelectric power generation at temperatures >600° in 1964 due to its stability with respect to oxidation, sublimation, evaporation and presence of non-toxic elements [1]. The typical ZT for $FeSi_2$ is 0.19 at 650 °C [1]. The $FeSi_2$ can be made n- or p-type by doping with Co (at Fe site) or Al (at Si site) [91]. TEGs have been fabricated using iron or $TiSi_2$ as interconnect material, which were bonded to $FeSi_2$ using $FeGe_2$ or Ti activated solder at hot end and ρ_c of as low as ~6×10^{-4} Ω cm^2 was reported [1,92]. At cold end, the contacts were made by $PbAg_3$ solder, which yielded ρ_c of ~1.3×10^{-4} Ω cm^2 [1]. Mg_2SiO_4 was used as filler in fabrication of $FeSi_2$ based TEGs. The best reported efficiency of TEGs fabricated using n-type $FeSi_2$ and p-type $MnSi_{1.72}$ was found to be ~3% for a ΔT ~ 600 °C and cold end temperature of 100 °C [1,93].

SiGe alloy is one of highly proven and efficient thermoelectric material for high temperature range of 800–1000 °C [1,2]. It can be easily made n and p-type by doping with phosphorus and boron, respectively. Since 1976, SiGe is the sole material which is being used as a power source in space mission [1]. At such high temperature of operation 800–1000 °C normally refractory metals such as W and Mo are used as interconnect materials [1,94]. In most of the literature, direct diffusion bonding of refractory metal, which form metal silicide at interface and results in contacts of low specific contact resistance (0.05 μΩ cm^2) is reported. As shown in Fig. 11, Taguchi et al. have used a buffer layer of carbon and Ni–Ag based brazing material for connecting SiGe thermoelements with the refractory metals interconnects and such an approach also yield very good electrical contacts [95]. The main role of carbon layer is two ways: (i) to reduce the thermal expansion mismatch of Mo layer with the SiGe and (ii) to avoid the direct contact of brazing material with the SiGe alloys. The typical voltage and power output from 9 p–n SiGe legs based TEG for respective hot and cold end temperatures of 553 °C and 44 °C is shown in Fig. 11(c).

During last few years, oxide based materials, such as $Ca_3Co_4O_9$, $NaCo_2O_4$, $CaMnO_3$, $LaNiO_3$, $SrTiO_3$, In_2O_3 and BiCuSeO have attracted lot of attention as thermoelectric material due to the ease of synthesis and low cost. These materials exhibit best thermoelectric performance at high temperatures >650 °C. Most oxide based TEG is currently fabricated using $Ca_3Co_4O_9$ or $NaCo_2O_4$-based material as p-type leg and $CaMnO_3$- or $LaNiO_3$-based material as

Table 3
Summary of various reported data for mid temperature (250–650 °C) range operating TEGs.

Thermoelements type	T_h/T_c	Interconnect material	Buffer layers at the ends	Efficiency (%)	Comments	Ref.
n-type PbTe p-type TAGS 85	500 °C/100 °C	Silver stripe	Ag/Fe/Ag + Fe	6	Formation of contacts by diffusion bonding	[81]
p-type ZnSb n-type Constantan	420 °C/20 °C			5.8	Direct joining of p and n type wires in the form of thermocouple	[90]
p- and n-type skutterudite	500 °C/40 °C	Aluminum	Molybdenum	7	Contact made by brazing	[87]
p & n type skutterudite	550 °C/70 °C		$CoSi_2$ for n-type and Co_2Si for p-type	9	Average ρ_c ~ 2 μΩ cm^2	[86]
p & n type skutterudite	550 °C/90 °C			10		[84]
n-type Bi_2Te_3/PbTe p-type Sb_2Te_3/PbTe	600 °C/10 °C	Copper	$Co_{0.8}Fe_{0.2}$ for PbTe side and Ni at Bi_2Te_3/Sb_2Te_3 sides	11	Segmented TEG, formation of contact by liquid In–Ga eutectic alloys	[85]

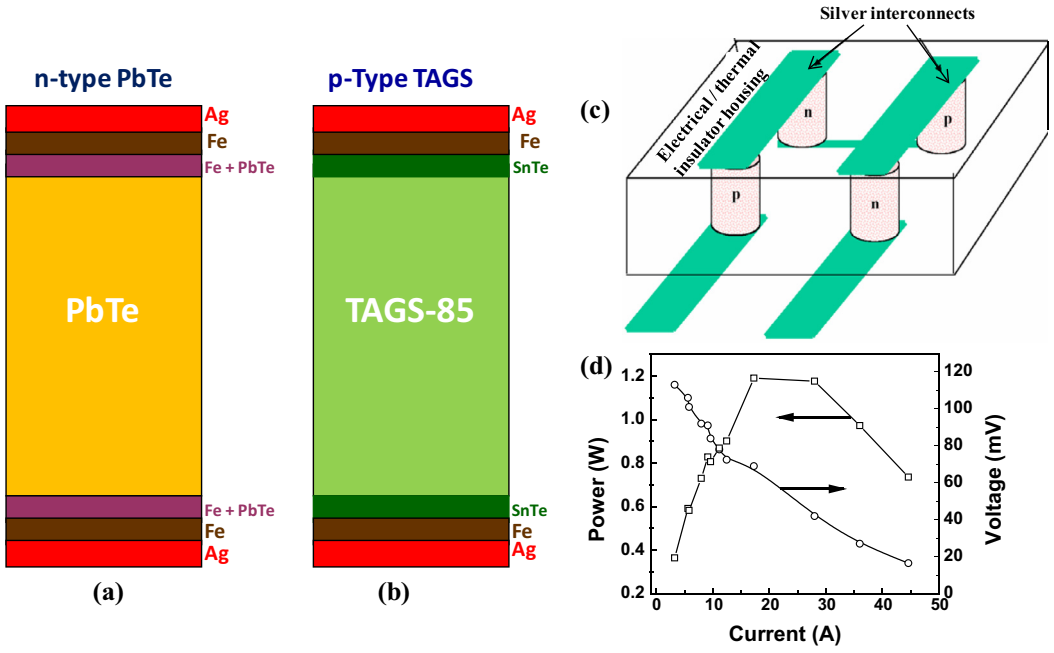

Fig. 9. Schematic of (a) n-type PbTe thermoelement and (b) TAGS-85 thermoelements with different buffer layers used for making low specific resistant electrical contact. (c) Schematic of a 2 p–n leg TEG fabricated using n –type PbTe and p-type TAGS-85 alloys. (d) The output power and load voltage across a match load resistance of 4 mΩ at hot side temperature of 500 °C and $\Delta T \sim 400$ °C [81].

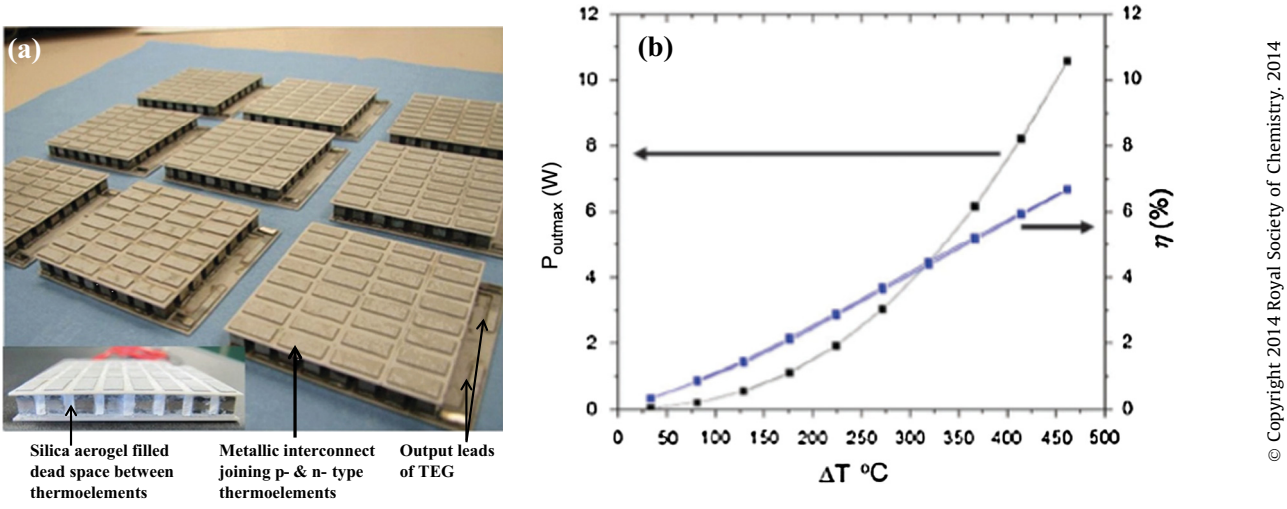

Fig. 10. (a) Photograph of the skutterdite (32 p–n couple) based TEG. The lower inset shows the same skutterdite TEG after silica aerogel encapsulation and (b) power output and efficiency as a function of ΔT for skutterudite based TEG for T_c of 40 °C. Reprinted with permission from Salvador et al. [87].

n-type leg. The performance of such TEG is much lower than expected because of several reasons: (i) high ρ_c at oxide/metal contact junctions; (ii) cracking or exfoliation due to the very different CTEs of oxide and metal; and (iii) the difficulty of having both p-type and n-type from the same parent compound. High working temperatures also make the conventional contact materials and fabrication procedures less viable. The first successful oxide TEG was fabricated using $Ca_3Co_4O_9$ as p-type thermoelement and $CaMnO_3$ as n-type thermoelements, which were joined using a copper strip with a mixture of silver paint and 6 wt.% oxide powder [98]. In this oxide based TEG, the contribution of contact resistance to the total internal resistance of the TEG was found to be around 22%. Ni and Fe–Cr alloy have also been tested as contact materials for $Ca_3Co_4O_9$. Although the Fe–Cr alloy was better than Ni, the reaction between the contact metals and the oxide at working temperature causes an increase of internal resistance. By introducing a buffer layer (consists of mixture of Ni and $SrRuO_3$ powders) in between Ni and $NaCo_2O_4$ helps to reduce the overall electrical resistivity [97]. In a recent report, an oxide-based TEG was fabricated using p-type $Ca_3Co_4O_9$ and n-type $(ZnO)_7In_2O_3$ legs [99]. The thermoelements were metallized by coating the ends with Ag paste and Ag wire was used as interconnect. A photograph of such an oxide based TEG with 8 p–n couples along with its power generation characteristics (with hot end at 1050 K) is shown in Fig. 12. In this study authors mentioned that open circuit voltage of the module was 54% of the theoretical value due to loss of voltage at the contacts. In summary although the oxide materials are considered to be environment friendly, they can be easily

Table 4
Summary of various reported data for TEG operating at high temperature range (>650 °C).

Thermoelements	T_h/T_c	Interconnect material	Buffer layers at the ends	Efficiency (%)	Comments	Ref.
n-$Fe_{0.93}Co_{0.07}Si_{1.99}Al_{0.01}$/p-$MnSi_{1.73}$	700 °C/100 °C	$TiSi_2$	–	3	Ti activated Ag solder used for joining, ρ_c at $FeSi_2$ leg ~80 μΩ cm^2 and ρ_c at $MnSi_{1.72}$ leg ~650 μΩ cm^2	[93]
n & p-type SiGe alloys	870 °C/31 °C	Molybdenum	Pressure contact	7	At low temperature end indium solder was used	[94]
n & p-type SiGe alloys	553 °C/44 °C	Molybdenum	Carbon	–	Formation of contact by Ni–Ag based brazing alloys	[95]
n & p-type SiGe alloys	1000 °C/300 °C	n & p type SiMo (i.e. $MoSi_2$ in the Si matrix) hot shoes connected with Ti layer	–	–	Diffusion bonding of SiMo hot shoe and W cold show with the thermoelements	[96]
n- type $Ca_{0.92}La_{0.08}MnO_3$ & p type $Ca_{2.75}Gd_{0.25}Co_4O_9$	773 °C /383 °C	n & p type elements connected via Pt wire	–	1.1	Thermoelements connected using Pt paste and ρ_c ~ 6.6 mΩ cm^2	[98]
Segmented leg of n-type ($La_{3-x}Te_4$/(Ba, Yb)Co_4Sb_{12}) and p-type ($Yb_{14}MnSb_{11}$/$Ce_{0.9}Fe_{3.5}Co_{0.5}Sb_{12}$)	1000 °C/152 °C	–	–	15		[101]
Segmented leg of p type [$Zn_{4-x}Cd_xSb_3$ + Zn_4Sb_3 + $(Bi/Sb)_2Te_3$] and n-type [$CoSb_3$ + $Bi_2(Te/Se)_3$]	700 °C/27 °C	–	–	15	Single leg device resistance ~2.79 mΩ with power output of 6.6 W	[102]
p-$Mg_2Si_{0.53}Sn_{0.4}Ge_{0.05}Bi_{0.02}$ and n-$MnSi_{1.75}Ge_{0.01}$	735 °C/50 °C	Mo on hot side and Cu on cold side	Ni/Pb/Ni on p-type and Cu on n-type	5.3	Spring loaded contact between thermoelements and metal interconnects, 12 p–n legs, output ~3.24 W, degradation of n-type thermoelement above 400 °C	[100]

synthesized, cheap in cost but still hunt for fabrication of efficient TEG is in progress, which depends on the development of the preparation of low ρ_c electrical contacts.

As discussed earlier, the TEG operating at high temperature range (>650 °C) and under large temperature gradient, exhibit low efficiency due to the low average *ZT* of the thermoelements. However, their efficiency can be improved by the use of segmented thermoelements. One of the classic examples of the segmented legs based TEG is demonstrated by Calliat et al. [101]. They have used segmented legs of n-type $La_{3-x}Te_4$/n-type (Ba, Yb)Co_4Sb_{12} and p-type $Yb_{14}MnSb_{11}$/p-type $Ce_{0.9}Fe_{3.5}Co_{0.5}Sb_{12}$ with hot end/cold end at 1000 °C/152 °C. The experimental efficiency of ~15% has been reported [101]. In another report by same group, by using a combination of state-of-the-art thermoelectric materials based on Bi_2Te_3 alloys and novel p-type Zn_4Sb_3, p-type $CeFe_4Sb_{12}$-based alloys and n-type $CoSb_3$-based alloys devices, they could achieve an efficiency of ~15% for hot side temperature of 700 °C and a cold side temperature of about 27 °C [102].

4. Cost considerations for the TEG developments

The development of TEG viable for commercial applications demands that they should be highly efficient and cost-effective [4,103,104]. LeBlanc et al. have reviewed the cost consideration of TEG development in detail by taking into account the raw materials prices, system components, manufacturing and optimized geometry [103]. Cost comparison of the best thermoelectric materials available for low, mid and high temperature ranges are given in Table 5.

For space and military applications, where the primary energy of the hot source has very high price, both the cost and weight of TEG are very important. In the case of free waste heat from sources e.g. exhaust of automobile, solar radiation, wind power, industrial furnaces, etc. the manufacturing cost of TEG becomes more important. Currently, all well-established TEGs are based on bismuth telluride, lead telluride and silicon germanium alloys, which require very expansive tellurium and germanium, and thus the

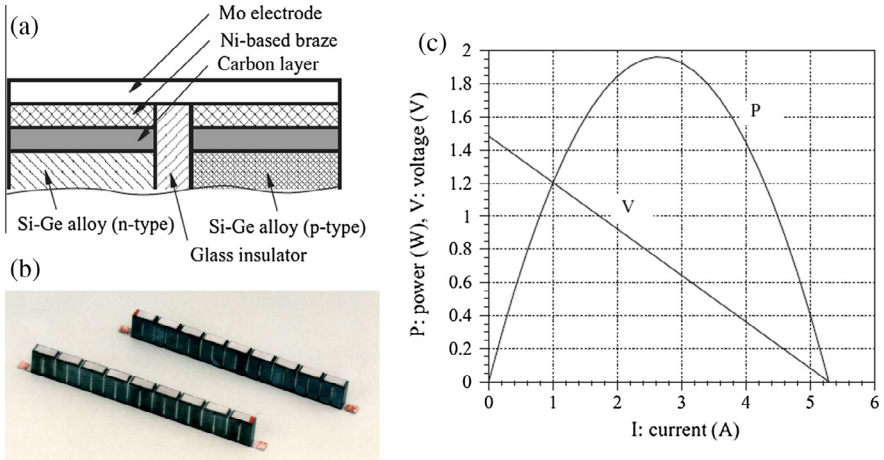

Fig. 11. (a) Details of the interface employed in the joining of thermoelements in the SiGe based TEG (b) photograph of linear shape SiGe module (c) voltage and power output from 9 p–n SiGe legs based TEG for respective hot and end temperatures of 553 °C and 44 °C [95].

cost of TEGs are very high. In order to reduce the cost of TEGs, efforts are being made to use inexpensive materials with relatively high *ZT*, and therefore, the current research is focused on materials like silicides, half Heuslers, oxides and organic materials.

It is evident from Table 5 that for low temperature range, conducting polymers (such as PEDOT:PSS) are the potential low-cost thermoelectric materials. However, the research on organic thermoelectric materials is at infancy and requires several issues before they become eligible for application in TEGs. These include higher *ZT*, long term stability, compatible metal interconnects, etc. For mid temperature TEGs, silicides are very cost effective but skutterdites may have edge because of their higher *ZT*. For high temperature TEGs, the bulk nanostructured silicon is highly competitive, but half-Heuslers compounds may find an edge due to higher *ZT* along with superior mechanical properties. It has been recently estimated that the cost of electricity generated by a TEG (i.e. around \$2 W^{-1}) fabricated using some novel class of thermoelectric materials can compete with the cost of electricity generated from other sources *viz.* natural gas (\$0.98 W^{-1}), coal (\$2.84 W^{-1}), nuclear (\$5.34 W^{-1}), geothermal (\$4.14 W^{-1}), etc. [4,103].

5. Applications of TEGs

TEG operating at different temperature range can have a variety of applications in communications, healthcare, aerospace, biomedical, remote power, military, etc. Some of these applications are briefly discussed.

5.1. TEG for societal applications

The communication and health care body-mounted electronic devices require a portable and autonomous energy source having an electrical power between 5 μW and 1 W with a life expectancy of ~5 years [104]. At present normal batteries are being used for such devices. These batteries usually contain the materials (such as sulfuric acid, mercury, zinc, lithium, lead, nickel and cadmium) which are not human friendly. The body-mounted flexible TEGs are alternative to such batteries, as they can be made using non-toxic materials. Body heat driven thermoelectric wrist watch is one of the commercialized example of body-mounted TEGs. Such TEG produces 300 mV of open-circuit voltage from a temperature gradient of 1.5 K with an efficiency of ~0.1%.

5.2. TEGs for waste heat recovery

TEGs can help to reduce the adverse effects of global warming by generating the electricity by harvesting waste heat which is by-product of industries, automobile engines and solar power. These freely available sources of waste heat are the main driving force behind the development of commercial TEGs for electricity generation. Several leading automobile manufacturers are developing TEG (having electrical power of ~1 kW) for waste heat recovery to improve the fuel economy of their automobiles [105]. Despite of low TEG efficiency, diligent harvesting of waste heat from resources such as automobile exhaust via judicious design and fabrication methods render TEGs as a worthwhile technology for the automobile manufacturers. A TEG with an efficiency of ~10% could be used to harvest 35–40% of the energy from the exhaust pipe (having average temperature of ~250 °C) to generate useable power that would contribute directly to the operation of the equipped vehicle, which could increase fuel efficiency by upto 16% [106]. In a recent study, 1 kW TEG system (based on n- and p-type half Heuslers) is experimentally demonstrated by recovering the exhaust waste heat from an automotive diesel engine. The TEG exhibited an efficiency of ~2.1% with ΔT of ~339 °C and exhaust temperature (T_h) ~ 550 °C [107].

5.3. TEGs as sensors

Conversion of heat into electrical signals by TEGs can be used as thermal-energy sensors such as cryogenic heat-flux sensors, water-condensation detectors, fluid-flow sensors, and infrared sensors [109]. Such thermal energy sensor has three important parameters as responsivity (i.e. ratio of the sensor voltage to the incoming radiation power), time constant and the noise voltage. However, in terms of size and light weight, the most effective structure for thermoelectric sensors are based on thin-films [110].

5.4. TEGs for space applications

In the deep space exploration missions (starts from mars and beyond it) the solar flux becomes so low that to generate a substantial electrical power, the size of solar panels become large. Hence for such space mission radio isotope thermoelectric generators (RTGs) have been used by the United States NASA to provide electrical power for spacecraft since 1961 [5]. In RTG, a general-purpose heat-source (GPHS) is used for heating, which is a composite carbon body that houses a radioactive pellet ($^{238}PuO_2$) and acts as an aero-impact shell. Such a protective shell is needed to avoid the spread of radioactive materials in case of failure. SiGe unicouples convert the heat generated by the radioactive decay of 238Pu in the $^{238}PuO_2$ fuel pellets. In some of the space mission by NASA, PbTe and TAGS-85 based n- and p-legs were used in RTGs.

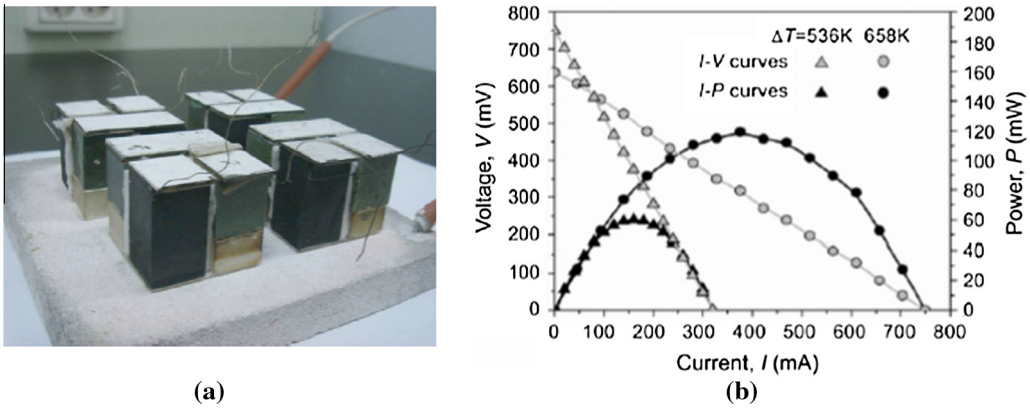

(a) (b)

Fig. 12. (a) Photograph of oxide based TEG consisting of 8 p–n couples and (b) power generation characteristics from oxide based TEG (shown in Fig. 12(a)) for a hot end temperature of 1050 K. Reprinted with permission from Choi et. al. [99]. Copyright 2011 Elsevier B.V.

Table 5
The cost of various thermoelectric materials according to Ref. [103].

Temperature range	Materials	Cost ($/kg)
Low (27–250 °C)	Bi_2Te_3	110
	$Bi_{0.52}Sb_{1.48}Te_3$	125
	Polymer (PEDOT:PSS)	0.43
Mid (250–650 °C)	$(Na_{0.0283}Pb_{0.945}Te_{0.9733})(Ag_{1.11}Te_{0.555})$	81
	$AgPb_{18}SbTe_{20}$	84
	$Yb_{0.2}In_{0.2}Co_4Sb_{12}$	24
	$CeFe_4Sb_{12}$	37
	$Ca_{0.18}Co_{3.97}Ni_{0.03}Sb_{12.40}$	13
	$Mg_2Si_{0.85}Bi_{0.15}$	6.67
	$Mg_2Si_{0.6}Sn_{0.4}$	4.04
	$MnSi_{1.75}$	1.46
	$Mn_{15}Si_{28}$	1.51
High (>650 °C)	$Zr_{0.25}Hf_{0.25}Ti_{0.5}NiSn_{0.994}Sb_{0.006}$	9.71
	$Zr_{0.5}Hf_{0.5}Ni_{0.5}Pd_{0.2}Sn_{0.99}Sb_{0.01}$	8.51
	$Ti_{0.8}Hf_{0.2}NiSn$	10.7
	SiGe	679
	Si	3.09
	$Ca_{2.4}Bi_{0.3}Na_{0.3}Co_4O_9$	30
	$Na_{0.7}CoO_{2-\delta}$	36

5.5. Solar TEG

One of the interesting applications of TEG is in producing electrical power from the heat generated by concentrating the solar energy [105,108]. Solar TEG basically uses a collector, TEG and a heat sink. The incident solar flux on the hot end of TEG can be varied with several collector options available such as evacuated flat plate, parabolic troughs, Fesnel lenses and parabolic discs. The efficiency of solar TEG is the product of optical to thermal conversion and TEG efficiency. So far the state-of-the-art solar TEG systems have achieved efficiency of ~5% for a temperature difference of about 100 °C with the materials of $ZT \sim 1$ [111]. Thus the major commercial barrier of solar TEG technology was its conversion efficiency, which is much lower than other solar electricity technologies such as solar cells exhibiting efficiency of ~18%. With the improvement in of *ZT* in various thermoelectric materials and improved design of solar collectors, high conversion efficiencies are expected in the future.

6. Perspective

The development a TEGs having efficiencies comparable to that of theoretical values have several technological challenges. The first requirement is the availability of p- and n-type materials with high *ZT* over a broad temperature range (decided by the hot and cold end temperature of TEG). The *ZT* can be enhanced either by improving the power factor and/or reduction of thermal conductivity for which several new approaches have been discovered. The basic idea behind the improvement of *ZT* is that the material should efficiently transport electrons, while significantly scattering the heat carrying phonons. Recently by integrating different approaches, *ZT* approaching to 2 has been obtained in different materials. For low temperatures (<250 °C), the best reported *ZT* of ~1.86 at 47 °C has been achieved in $Bi_{0.5}Sb_{1.5}Te_3$. For mid temperature range (250–650 °C), the best reported *ZT* of ~ 2.2 at 642 °C has been obtained in PbTe-SrTe solid solutions based bulk nanostructures. For high temperature range (> 650 °C), the best *ZT* of 1.8 at 800 °C has been obtained for n-type SiGe alloys. The second requirement for TEG development is joining the p- and n-type thermoelements by an appropriate metallic interconnect with specific contact resistance (between thermoelements and interconnects) of <1 $\mu\Omega\,cm^2$. So far the best reported average specific contact resistance of ~1 $\mu\Omega\,cm^2$ has been reported for Bi_2Te_3 thermoelements modified with self-assembled 3-mercapto propyl-trimethoxysilane. For long term stability of devices, thermal expansion coefficient of interconnect materials should match with thermoelectric materials, which in practice difficult to obtain. Thus, an appropriate buffer layer with intermediate thermal expansion coefficient is normally introduced between the interconnect and thermoelement. Such buffer layers are either a different material or a graded layer consisting of thermoelectric and interconnect material. Since TEGs operate at a large temperature gradient, therefore it is also important to ensure that no diffusion

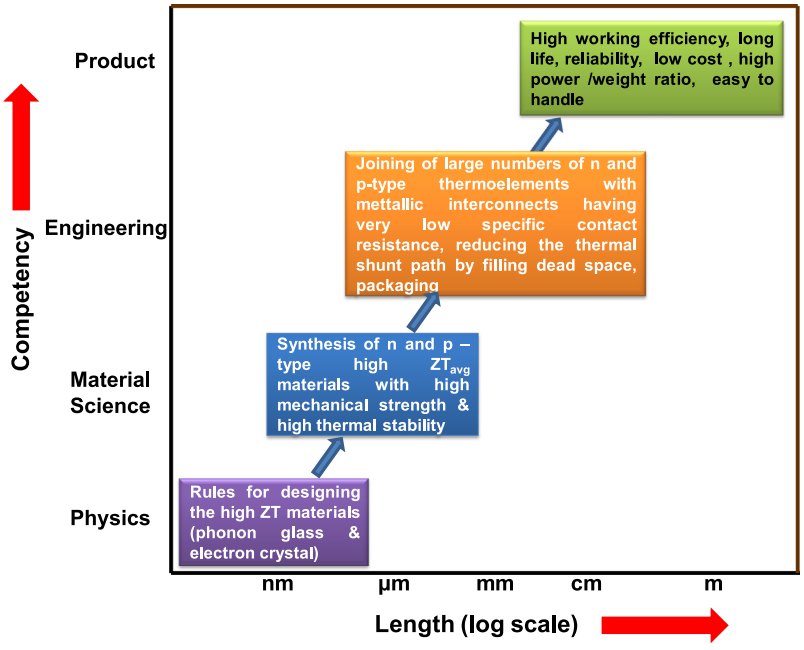

Fig. 13. Schematic representation of technology development of thermoelectric power generators requiring competence at multidisciplinary sciences at different length scales.

of buffer layer or interconnect takes place into thermoelectric materials that would degrade thermoelectric properties in a longer run. The third and important requirement for TEG development is to avoid direct flow of heat from the hot surface to cold surface through the dead volume between thermoelements. Low thermal conductivity materials such as silica based aerogel, zirconia based ceramics etc. have been used to obstruct the direct flow of heat from hot to cold end. As the expected life span for TEGs is several years therefore it need to be ensured that no part of the device undergoes a degradation. In addition, the materials used in TEGs should be environmental friendly, low cost, long chemically stable, scalable for mass production with and high mechanical strength. To sum up, as schematically depicted in Fig. 13, the technology development of efficient TEG requires competence at multidisciplinary sciences i.e. physics, materials science, engineering and product development, which need to be executed at different length scales. It is expected that economically viable TEGs will see the commercial applications in very near future.

7. Summary

In this short review we have discussed the challenges associated at different levels in the development of efficient TEGs. The major challenges can be divided into three different areas: (i) High figure-of-merit environment friendly thermoelectric materials for operation at different temperatures. A significant amount of research has already been done in this direction and materials exhibiting *ZT* close to 2 have been synthesized, using novel concepts. These includes either (a) improving the power factor without affecting thermal transport through creation multiple valley band structure, electronic resonance states, modulation doping, depressing bipolar effect etc. (b) reducing the lattice thermal conductivity without compromising the power factor by scattering efficiently the phonons using scale hierarchical structures created in the material. Apart from the availability of n- and p- type materials with high *ZT* another important issue is the preparation of ohmic contacts of metallic interconnects with p- and n-type thermoelements having very low specific contact resistances. Obviously these studies are materials specific and in some cases very low contact resistances have been obtained using appropriate buffer layers. However, more studies need to be carried out in future, in particularly for those materials which are environmental friendly, exhibiting high *ZT*, stability and low cost. (iii) Packaging of the TEGs with minimal thermal shunt between hot and cold sides of the devices. This aspect has not been given importance in the literature, though some low thermal conductivity materials like asbestos, silica based aerogel, zirconia based ceramics etc. have been utilized. A detail theoretical modeling of heat flow though TEGs along with selection of appropriate heat blocking materials requires to be carried out. It is believed that with industry taking part in the manufacturing of TEGs along with increased scientific and engineering interests in these devices, the commercial applications of TEGs is feasible in very near future.

Acknowledgements

The authors would like to thank Dr. S.K. Gupta, Dr. Shovit Bhattacharya, Dr. Ranu Bhatt, Mr. Sajid Ahmad, Mr. K.N. Meshram and Professor Y. Hayakawa for providing their support and valuable inputs for this article. Dr. D.K. Aswal would like to thank the cooperative research project of the Research Institute of Electronic, Shizuoka University.

References

[1] Rowe DM. In: Rowe DM, editor. Thermoelectrics handbook. Boca Raton (FL): CRC Press; 1995.
[2] Bhandari CM, Rowe DM. Modern thermoelectrics. Virginia: Reston Publishing Company; 1983.
[3] Zevenhovena R, Beyeneb A. The relative contribution of waste heat from power plants to global warming. Energy 2011;36:3754–62.
[4] LeBlanc S. Thermoelectric generators: linking material properties and systems engineering for waste heat recovery applications. Sustain Mater Technol 2014;1–2:26–35.
[5] https://solarsystem.nasa.gov/rps/rtg.cfm.
[6] Zhao Li-D, Dravid VP, Kanatzidis MG. The panoscopic approach to high Performance thermoelectric. Energy Environ Sci 2014;7:251–68.
[7] Snyder GJ, Toberer ES. Complex thermoelectric materials. Nat Mater 2008;7:105.
[8] Liu W, Jie Q, Kim HS, Ren Z. Current progress and future challenges in thermoelectric power generation: from materials to devices. Acta Mater 2015;87:357–76.
[9] Zebarjadi M, Esfarjani K, Dresslhaus MS, Ren ZF, Chen G. Perspectives on thermoelectrics: from fundamentals to device applications. Energy Environ Sci 2012;5:5147–62.
[10] Chen Z-G, Han G, Yang L, Cheng L, Zou J, Gang, et al. Nanostructured thermoelectric materials: current research and future challenge. Progr Nat Sci: Mater Int 2012;6:535–49.
[11] Rull-Bravo M, Moure A, Fernandez JF, Martín-González M. Skutterudites as thermoelectric materials: revisited. RSC Adv 2015;5:41653–67.
[12] Snyder GJ. Application of the compatibility factor to the design of segmentedand cascaded thermoelectric generators. Appl Phys Lett 2004;84:2436–8.
[13] Snyder GJ, Ursell TS. Thermoelectric efficiency and compatibility. Phys Rev Lett 2003;91:148301–4.
[14] Pei Y, Shi X, LaLonde A, Wang H, Chen L, Snyder GJ. Convergence of electronic bands for high performance bulk thermoelectric. Nature 2011;473:66–9.
[15] Pei Y, Wang H, Snyder GJ. Band engineering of thermoelectric materials. Adv Mater 2012;24:6125–35.
[16] Hermans JP, Wiendlocha B, Chamoire AM. Resonant levels in bulk thermoelectric semiconductors. Energy Environ Sci 2012;5:5510–30.
[17] Levin EM, Bud'ko SL, Schmidt-Rohr K. Enhancement of thermopower of TAGS-85 high-performance thermoelectric material by doping with the rare earth Dy. Adv Funct Mater 2012;22:2766–74.
[18] He M, Ge J, Lin Z, Feng X, Wang X, Lu H, et al. Thermopower enhacement in the conducting polymer nanocomposites via carrier energy scattering at the organic–inorganic semiconductor interface. Energy Environ Sci 2012;5:8351–8.
[19] Lee JH, Wu J, Grossman JC. Enhancing the thermoelectric power factor with highly mismatched isoelectronic doping. Phys Rev Lett 2010;104(16):602–3.
[20] Yu B, Zebarjadi M, Wang H, Lukas K, Wang H, Wang D, et al. Enhancement of thermoelectric properties by modulation-doping in silicon germanium alloy nanocomposites. Nano Lett 2012;12:2077–82.
[21] Zebarjadi M, Joshi G, Zhu G, Yu B, Minnich A, Lan Y, et al. Power factor enhancement by modulation doping in bulk nanocomposites. Nano Lett 2011;11:2225–30.
[22] He J, Kanatzidis MG, Dravid VP. High performance bulk thermoelectric via a panoscopic approach. Mater Today 2013;16:166–76.
[23] Zhao LD, Wu HJ, Hao SQ, Wu CI, Zhou XY, Biswas K, et al. All-scale hierarchical thermoelectrics: MgTe in PbTe facilitates valence band convergence and suppresses bipolar thermal transport for high performance. Energy Environ Sci 2013;6:3346–55.
[24] Kittel C. Introduction to solid state physics, 8th ed.; 2005 [ISBN 0-471-41526-X].
[25] Slack GA. The thermal conductivity of nonmetallic crystals. Solid State Phys 1979;34:1–71.
[26] Biswas K, He J, Blum ID, Wu CI, Hogan TP, Seidman DN, et al. High-performance bulk thermoelectrics with all-scale hierarchical architectures. Nature 2012;489:414–8.
[27] Chung D-Y, Hogan T, Brazis P, Rocci-Lane M, Kannewurf C, Bastea M, et al. $CsBi_4Te_6$: a high-performance thermoelectric material for low-temperature applications. Science 2000;287:1024–7.
[28] Jin H, Jaworski CM, Hereman JP. Enhancement in the figure of merit of p-type BiSb alloys through multiple valence-band doping. Appl Phys Lett 2012;101:053904.
[29] Chen Z, Zhou M, Huang RJ, Song CM, Zhou Y, Li LF. Thermoelectric properties of p-type Pb-doped $Bi_{85}Sb_{15-x}Pb_x$ alloys at cryogenic temperatures. J Alloys Compd 2012;511:85–9.
[30] Hu L-P, Zhu T-J, Wang Y-G, Xie H-H, Xu Z-J, Zhao X-B. Shifting up the optimum figure of merit of p-type bismuth telluride-based thermoelectric materials for power generation by suppressing intrinsic conduction. NPG Asia Mater 2014;6(e88):1–8. http://dx.doi.org/10.1038/am.2013.86.
[31] Jiang Q, Yan H, Khaliq J, Ning H, Grasso S, Simpson K, et al. Large ZT enhancement in hot forged nanostructured p-type $Bi_{0.5}Sb_{1.5}Te_3$ bulk alloys. J Mater Chem A 2014;2:5785–90.
[32] Bubnova O, Khan ZU, Malti A, Braun S, Fahlman M, Berggren M, et al. Optimization of the thermoelectric figure of merit in the conducting polymer

poly(3,4ethylenedioxythiophene). Nat Mater 2011;10:429433. http://dx.doi.org/10.1038/nmat3012.
[33] Sun Y, Sheng P, Di C, Jiao F, Xu W, Qiu D, et al. Organic thermoelectric materials and devices based on p- and n-type poly(metal 1,1,2,2-ethenetetrathiolate)s. Adv Mater 2012;24:932–7.
[34] Kim G-H, Shao L, Zhang K, Pipe KP. Engineered doping of organic semiconductors for enhanced thermoelectric efficiency. Nat Mater 2013;12:719–23.
[35] Liu H, Yuan X, Lu P, Shi X, Xu F, He Y, et al. Ultrahigh thermoelectric performance by electron and phonon critical scattering in $Cu_2Se_{1-x}I_x$. Adv Mater 2013;25:6607–12. http://dx.doi.org/10.1002/adma.20130266.
[36] Wojciechowski KT, Schmidt M. Structural and thermoelectric properties of $AgSbTe_2$–$AgSbSe_2$ pseudobinary system. Phys Rev B 2009;79:184202–4. http://dx.doi.org/10.1103/PhysRevB.79.184202.
[37] Hsu KF, Loo S, Guo F, Chen W, Dyck JS, Uher C, et al. Cubic $AgPb_mSbTe_{2+m}$: bulk thermoelectric materials with high figure of merit. Science 2004;303:818–21.
[38] Liu W, Tan X, Yin K, Liu H, Tang X, Shi J, et al. Convergence of conduction bands as a means of enhancing thermoelectric performance of n-type $Mg_2Si_{1-x}Sn_x$ solid solutions. Phys Rev Lett 2012;108:166601–3.
[39] Bux SK, Yeung MT, Toberer ES, Snyder GJ, Kaner RB, Fleurial Jean-Pierre. Mechanochemical synthesis and thermoelectric properties of high quality magnesium silicide. J Mater Chem 2011;21:12259–66. http://dx.doi.org/10.1039/C1JM10827A.
[40] Khan AU, Vlachos N, Kyratsi Th. High thermoelectric figure of merit of $Mg_2Si_{0.55}Sn_{0.4}Ge_{0.05}$. Scr Mater 2013;69:606–9.
[41] Itoh T, Yamada M. Synthesis of thermoelectric manganese silicide by mechanical alloying and pulse discharge sintering. J Electr Mater 2009;38:925–9.
[42] Luo W, Li H, Yan Y, Lin Z, Tang X, Zhang Q, et al. Rapid synthesis of high thermoelectric performance higher manganese silicide with in-situ formed nano-phase of MnSi. Intermetallics 2011;19:404–8.
[43] Bhattacharya S, Basu R, Bhatt R, Pitale S, Singh A, Aswal DK, et al. $CuCrSe_2$: a high performance phonon glass and electron crystal thermoelectric material. J Mater Chem A 2013;1:11289–94.
[44] Gascoin F, Maignan A. Order-disorder transition in AgCrSe2: a new route to efficient thermoelectrics. Chem Mater 2011;23:2510–3.
[45] Bhattacharya S, Bohra A, Basu R, Bhatt R, Ahmad S, Meshram KN, et al. High thermoelectric performance of $(AgCrSe_2)_{0.5}(CuCrSe_2)_{0.5}$ nano-composites having all-scale natural hierarchical architectures. J Mater Chem A 2014;2:17122–9.
[46] Zhao Li-Dong, Hao S, Lo Shih-Han, Wu Chun-I, Zhou X, Lee Y, et al. High thermoelectric performance via hierarchical compositionally alloyed nanostructures. J Am Chem Soc 2013;135:7364–70.
[47] Zhao Li-Dong, Lo Shih-Han, Zhang Y, Sun H, Tan G, Uher C, et al. Ultralow thermal conductivity and high thermoelectric figure of merit in SnSe crystals. Nature 2014;508:373–7.
[48] Shi X, Yang J, Salvador JR, Chi M, Cho JY, Wang H, et al. Multiple-filled skutterudites: high thermoelectric figure of merit through separately optimizing electrical and thermal transports. J Am Chem Soc 2011;133:7837–46.
[49] Liu WS, Zhang BP, Zhao LD, Li LF. Improvement of thermoelectric performance of $CoSb_{3-x}Te_x$ skutterudite compounds by additional substitution of IVB-group elements for Sb. Chem Mater 2008;20:7526–31.
[50] Duan B, Zhai P, Liu L, Zhang Q, Ruan X. Synthesis and high temperature transport properties of Te-doped skutterudite compounds. J Mater Sci: Mater Electron 2012;23:1817–22.
[51] Su X, Li H, Wang G, Chi H, Zhou X, Tang X, et al. Structure and transport properties of double-doped $CoSb_{2.75}Ge_{0.25-x}Te_x$ ($x = 0.125–0.20$) with in situ nanostructure. Chem Mater 2011;23:2948–55.
[52] Xu C, Duan B, Ding S, Zhai P, Zhang Q. Thermoelectric properties of skutterudites $Co_{4-x}Ni_xSb_{11.9-y}Te_ySe_{0.1}$. J Electron Mater 2014;43:2224–8.
[53] Fleurial JP, Borshchevsky A, Cailliat T, Morelli DT, Meisner GP. Thermoelectrics. Fifteenth international conference; 1996.
[54] Tang X, Zhang Q, Chen L, Goto T, Hirai T. Synthesis and thermoelectric properties of p-type- and n-type-filled skutterudite $R_yM_xCo_{4-x}Sb_{12}$ (R: Ce, Ba, Y; M:Fe, Ni). J Appl Phys 2005;97:093712.
[55] Rogl G, Grytsiv A, Bauer E, Rogal P, Zhetbauer M. Thermoelectric properties of novel skutterudites with didymium: $DD_y(Fe_{1-x}Co_x)_4Sb_{12}$ and $DD_y(Fe_{1-x}Ni_x)_4Sb_{12}$. Intermetallics 2010;18:57–64.
[56] Rogl G, Grytsiv A, Heinrich P, Bauer E, Kumar P, Peranio N, et al. New bulk p-type skutterudites $DD_{0.7}Fe_{2.7}Co_{1.3}Sb_{12}-xXx$ (X = Ge, Sn) reaching ZT > 1.3. Acta Mater 2015;91:227–38.
[57] Liu FS, Zheng JX, Huang MJ, He LP, Ao WQ, Pan F, et al. Enhanced thermoelectric performance of $Cu_2CdSnSe_4$ by Mn doping: experimental and first principles studies. Sci Rep 2014;4:5774. http://dx.doi.org/10.1038/srep0577.
[58] Liu M-L, Huang F-Q, Chen L-D, Chen I-W. A wide-band-gap p-type thermoelectric material based on quaternary chalcogenides of Cu_2ZnSnQ_4, Q = S, Se. Appl Phys Lett 2009;94:202103.
[59] Shi XY, Huang FQ, Liu ML, Chen LD. Thermoelectric properties of tetrahedrally bonded wide-gap stannite compounds $Cu_2ZnSn_{1-x}In_xSe_4$. Appl Phys Lett 2009;94:122103.
[60] Joshi G, Dahala T, Chena S, Wanga H, Shiomi J, Chen G, et al. Enhancement of thermoelectric figure-of-merit at low temperatures by titanium substitution for hafnium in n-type half-Heuslers $Hf_{0.75-x}Ti_xZr_{0.25}NiSn_{0.99}Sb_{0.01}$. Nano Energy 2013;2:82–7.
[61] Liu Y, Poudeu PFP. Thermoelectric properties of Ge doped n-type $Ti_xZr_{1-x}NiSn_{0.975}Ge_{0.025}$ half-Heusler alloys. J Mater Chem A 2015;3:12507–14.
[62] Fu C, Zhu T, Liu Y, Xie H, Zhao X. Band engineering of high performance p-type FeNbSb based half-Heusler thermoelectric materials for figure of merit $ZT > 1$. Energy Environ Sci 2015;8:216–20.
[63] Joshi G, He R, Engber M, Samsonidze G, Pantha T, Dahal E, et al. NbFeSb-based p-type half-Heuslers for power generation applications. Energy Environ Sci 2014;7:4070–6.
[64] Sahoo P, Liu Y, Makongo JPA, Su Xian-Li, Kim SJ, Takas N, et al. Enhancing thermopower and hole mobility in bulk p-type half-Heuslers using full-Heusler nanostructure. Nanoscale 2013;5:9419–27.
[65] Zho L-D, He J, Hao S, Wu C-I, Hogan TP, Wolverton C, et al. Raising the thermoelectric performance of p-Type PbS with endotaxial nanostructuring and valence-band offset engineering using CdS and ZnS. J Am Chem Soc 2012;134:16327–36.
[66] Basu R, Bhattacharya S, Bhatt R, Roy M, Ahmad S, Singh A, et al. Improved thermoelectric performance of hot pressed nanostructured n-type SiGe bulk alloys. J Mater Chem A 2014;2:6922–30.
[67] Bathula S, Mula J, Bhasker BG, Singh NK, Tyagi K, Srivastava AK, et al. Role of nanoscale defect features in enhancing the thermoelectric performance of p-type nanostructured SiGe alloys. Nanoscale 2015. http://dx.doi.org/10.1039/C5NR01786F.
[68] Wang C, Lin S, Chen H, Zhao Y, Zhao L, Wang H, et al. Thermoelectric performance of $Si_{80}Ge_{20-x}Sb_x$ based multiphase alloys with inhomogeneous dopant distribution. Energy Convers Manage 2015;94:331–6.
[69] Brown SR, Kauzlarich SM, Gascoin F, Snyder GJ. $Yb_{14}MnSb_{11}$: new high efficiency thermoelectric material for power generation. Chem Mater 2006;1:1873–7.
[70] May AF, Fleurial J-P, Snyder GJ. Optimizing thermoelectric efficiency in $La_{3-x}Te_4$ via Yb substitution. Chem Mater 2010;22:2995–9.
[71] Sui J, Li J, He J, Pei Y-L, Berardan D, Wu H, et al. Texturation boosts the thermoelectric performance of BiCuSeO oxyselenides. Energy Environ Sci 2013;6:2916–20.
[72] Liu H, Shi X, Xu F, Zhang L, Zhang W, Chen L, et al. Copper ion liquid like thermoelectric. Nat Mater 2012;11:422–5.
[73] Gahtori B, Bathula S, Tyagi K, Jayasimhadri M, Srivastava AK, Singh S, et al. Giant enhancement in thermoelectric performance of copper selenide by incorporation of different nanoscale dimensional defect features. Nano Energy 2015;3:36–46.
[74] Xiong K, Wang W, Alshareef HN, Gupta RP, White JB, Gnade BE, et al. Electronic structures and stability of Ni/Bi_2Te_3 and Co/Bi_2Te_3 interfaces. J Phys D Appl Phys 2010;43:115303–6.
[75] Liu WS, Wang HZ, Wang LJ, Wang XW, Joshi G, Chen G, et al. Understanding of the contact of nanostructured thermoelectric n-type $Bi_2Te_{2.7}Se_{0.3}$ legs for power generation applications. J Mater Chem A 2013;1:13093–100.
[76] Feng SP, Chang YH, Yang J, Poudel B, Yu B, Ren ZF, et al. Reliable contact fabrication on nanostructured Bi_2Te_3-based thermoelectric materials. Phys Chem Chem Phys 2013;15:6757–62.
[77] Sun Y, Sheng P, Di Chongan, Jiao F, Xu W, Qiu D, et al. Organic thermoelectric materials and devices based on p- and n-type poly(metal 1,1,2,2-ethenetetrathiolate)s. Adv Mater 2012;24:932–7.
[78] Muto A, Kraemer D, Hao Q, Ren ZF, Chen G. Thermoelectric properties and efficiency measurements under large temperature differences. Rev Sci Instrum 2009;80:093901–93907.
[79] Kraemer D, Sui J, McEnaney K, Zhao H, Jie Q, Ren ZF, et al. High thermoelectric conversion efficiency of MgAgSb-based material with hot-pressed contacts. Energy Environ Sci 2015;8:1299–308.
[80] Li CC, Drymiotis F, Liao LL, Dai MJ, Liu CK, Chen CL, et al. Silver as a highly effective bonding layer for lead telluride thermoelectric modules assembled by rapid hot-pressing. Energy Convers Manage 2015;98:134–7.
[81] Singh A, Bhattacharya S, Thianaharan C, Aswal DK, Gupta SK, Yakhmi JV, et al. Development of low resistance electrical contacts for thermoelectric devices based on n-type PbTe and p-type TAGS-85 $((AgSbTe_2)_{0.15}(GeTe)_{0.85})$. J Phys D Appl Phys 2009;42:015502–15506.
[82] Cailliat T, Fleurial JP, Snyder GJ, Borshchevsky. Development of high efficiency segmented thermoelectric unicouples. In: Proc of 20th international conf on thermoelectrics; 2001. p. 282–5.
[83] Fleurial JP, Caillat T, Chi SC. Electrical contacts for skutterudite thermoelectric materials. US patent US 2012/0006376 A1; 2012.
[84] Guo JQ, Geng HY, Ochi T, Suzuki S, Kikuchi M, Yamaguchi S, et al. Development of skutterudite thermoelectric materials and modules. J Electron Mater 2012;41:1036–42.
[85] Hu X, Jood P, Ohta M, Kunii M, Nagase K, Nishiate H, et al. Power generation from nanostructured PbTe-based thermoelectrics: comprehensive development from materials to modules. Energy Environ Sci 2015. http://dx.doi.org/10.1039/c5ee02979a.
[86] Muto A, Yang J, Poudel B, Ren ZF, Chen G. Skutterudite unicouple characterization for energy harvesting applications. Adv Energy Mater 2013;3:245–51.
[87] Salvador JR, Cho JY, Ye Z, Moczygemba JE, Thompson AJ, Sharp JW, et al. Conversion efficiency of skutterudite-based thermoelectric modules. Phys Chem Chem Phys 2014;16:12510–20.
[88] Nemoto T, Iida T, Sato J, Saakamoto T, Hirayamo N, Nakajima T, et al. Development of an Mg_2Si unileg thermoelectric module using durable Sb-doped Mg_2 Si Legs. J Electron Mater 2013;42:2192–7.

[89] de Boor J, Gloanec C, Kolb H, Sottong R, Ziolkowski P, Müller E. Fabrication and characterization of nickel contacts for magnesium silicide based thermoelectric generators. J Alloys Compd 2015;632:348–53.
[90] Telkes M. Solar thermoelectric generators. J Appl Phys 1954;25:765–7.
[91] Birkholz U. Iron silicide as thermoelectric generator material. In: Scherrer H, Scherrer S, editors, Proc 8th int conf thermoelectric energy conversion. Nancy (France): Institute National Polytechnique de Lorraine; 1989. p. 151.
[92] Birkholz U, Groβ E, Riffel M, Roth H, Stöhrer U, Wittmer W. Measurement of the efficiency of a HMS-$FeSi_2$ thermoelectric generator. In: Rao KR, editors, Proc 11th int conf on thermoelectric energy conversion. Arlington: University of Texas; 1992. p. 51.
[93] Groβ E, Riffel M, Stöhrer U. Thermoelectric generators made of $FeSi_2$ and HMS: fabrication and measurement. J Mater Res 1995;10:34–40.
[94] Abels B, Cohen RB. Ge–Si thermoelectric power generators. J Appl Phys 1964;35:247–8.
[95] Taguchi K, Terakado K, Ogusu M, Matumoto A, Kayamoto T, Okura K, et al. Linear shaped Si–Ge thermoelectric module. In: Seoul 2000 FISITA world automotive congress, F2000A045, June 12–15, 2000, Seoul, Korea; 2000.
[96] Nakahara JF, Franklin B, DeFillipo LE. Development of an improved performance SiGe unicouple. AIP Conf Proc 1995;324:809.
[97] Arai K, Matsubara M, Swada Y, Sakamoto T, Kineri T, Kogo Y, et al. Improvement of electrical contact between TE material and Ni electrode interfaces by application of a buffer layer. J Electron Mater 2012;41:1771–7.
[98] Matsubara I, Funahashi R, Takeuchi T, Sodeoka S, Shimizu T, Ueono K. Fabrication of an all-oxide thermoelectric power generator. Appl Phys Lett 2001;78:3627–9.
[99] Choi SM, Lee KH, Lim CH, Seo WS. Oxide-based thermoelectric power generation module using p-type $Ca_3Co_4O_9$ and n-type $(ZnO)_7In_2O_3$ legs. Energy Convers Manage 2011;52:335–9.
[100] Skomedal G, Holmgren L, Middleton H, Eremin IS, Isachenko GN, Jaegle M, et al. Design, assembly and characterization of silicide-based thermoelectricmodules. Energy Convers Manage 2016;110:13–21.
[101] Caillat T, Firdosy S, Cheng B, Paik J, Chase J, Arakelian T, et al. Proc Nucl Emerg Technol Space 2012:3077.
[102] Caillat T, Borshchevsky A, Snyder J, Fleurial JP. High efficiency segmented thermoelectric unicouples. AIP Conf Proc 2001;552:1107–12.
[103] LeBlanc S, Yee SK, Scullin ML, Dames C, Goodson KE. Material and manufacturing cost considerations for thermoelectrics. Sustain Energy Rev 2014;32:313–27.
[104] Schierning G, Chavez R, Schmechel R, Balke B, Rogl G, Rogl P. Concepts for medium-high to high temperature thermoelectric heat-to-electricity conversion: a review of selected materials and basic considerations of module design. Transl Mater Res 2015;2:025001–25026.
[105] Elsheikh MM, Shnawah DA, Sabri MFM, Said SBM, Hassan MH, Bashir MBA, et al. A review on thermoelectric renewable energy: principle parameters that affect their performance. Renew Sustain Energy Rev 2014;30:337–55.
[106] Yu C, Chau KT. Thermoelectric automotive waste heat energy recovery using maximum power point tracking. Energy Convers Manage 2009;50:1506–12.
[107] Zhang Y, Cleary M, Wang X, Kempf N, Schoensee L, Yang J, et al. High-temperature and high-power-density nanostructured thermoelectric generator for automotive waste heat recovery. Energy Convers Manage 2015;105:946–50.
[108] Sundarraj P, Maity D, Roy SS, Taylor RA. Recent advances in thermoelectric materials and solar thermoelectric generators – a critical review. RSC Adv 2014;4:46860–74.
[109] Kockmann N. Encyclopedia of Microfluidics and Nanofluidics. New York: Springer Science Business Media; 2013. http://dx.doi.org/10.1007/978-3-642-27758-0-1577-4.
[110] Yang Y, Lin Z-H, Hou T, Zhang F, Wang ZL. Nanowire-composite based flexible thermoelectric nanogenerators and self-powered temperature sensors. Nano Res 2012;5:888–95.
[111] Kraemer D, Poudel B, Feng H-P, Caylor JC, Yu B, Yan X, et al. High-performance flat-panel solar thermoelectric generators with high thermal concentration. Nat Mater 2011;10:532–8.